70. J. R. Engen, T. E. Wales, Analytical Aspects of Hydrogen Exchange Mass Spectrometry. *Annu. Rev. Anal. Chem.* **8**, 150605180052009 (2015).
71. D. Houde, S. A. Berkowitz, J. R. Engen, The utility of hydrogen/deuterium exchange mass spectrometry in biopharmaceutical comparability studies. *J. Pharm. Sci.* **100**, 2071--2086 (2011).
72. L. A. Diaz-Martinez, Y. Kang, K. J. Walters, D. J. Clarke, Yeast UBL-UBA proteins have partially redundant functions in cell cycle control. *Cell Div.* **1**, 28 (2006).
73. F. Geng, W. P. Tansey, Similar temporal and spatial recruitment of native 19S and 20S proteasome subunits to transcriptionally active chromatin. *Proc. Natl. Acad. Sci. U. S. A.* **109**, 6060--6065 (2012).

ACKNOWLEDGMENTS

For advice, assistance, or comments on the manuscript, we thank D. Chandler-Militello, M. Gill, J. Hanna, A. Kajava, R. King, Y. Lu, Y. Li, M. Pahre, and J. Roelofs. For gifts of reagents we thank D. Clarke, M. Glickman, F. He, Y. Ye, D. Komander, C. Larsen, J. Li, U. Nowicka, S. Sadis, and W. Tansey. This research was funded by grants from the National Institutes of Health (R37-GM043601 to D.F., CA136472 to K.J.W., and R01-GM101135 to J.R.E.), by the Intramural Research Program of the NIH, National Cancer Institute, Center for Cancer Research to K.J.W., and by a research collaboration with the Waters Corporation (J.R.E). Atomic coordinates for the Rpn1 T1 site, Rpn1 T1:ubiquitin, and Rpn1 T1:K48 diubiquitin are available through the Protein Data Bank with accession codes 2n3t, 2n3u, and 2n3v/2n3w, respectively.

SUPPLEMENTARY MATERIALS

Figs. S1 to S34
Tables S1 to S5
References (*50-73)*

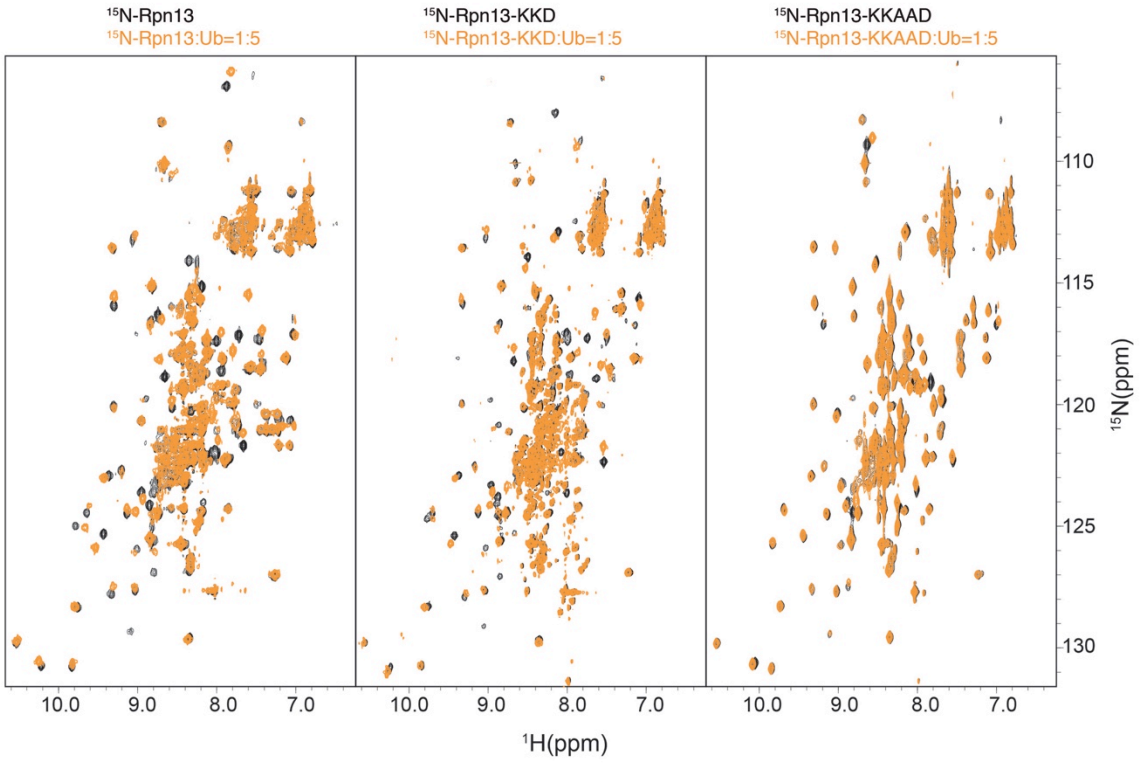

Fig. S1.

Resonance shifts in Rpn13 induced by ubiquitin are strongly attenuated in the Rpn13-KKAAD protein. ^{1}H, ^{15}N HSQC spectra of ^{15}N Rpn13 Pru domain wild-type (left), E41K/E42K/S93D (KKD, middle), and E41K/E42K/L43A/F45A/S93D (KKAAD, right) alone (black) and with unlabeled monoubiquitin at 5-fold molar excess (orange).

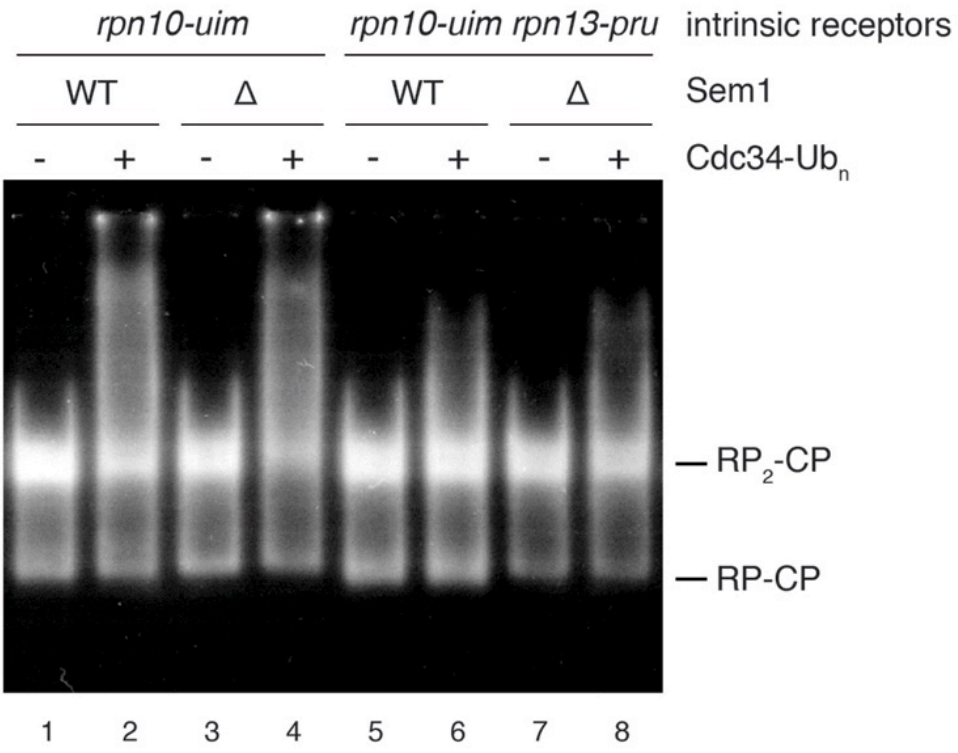

Fig. S2.

Assessment of Sem1 as a receptor for ubiquitin in the context of the proteasome. Proteasomes were purified as described from the strains listed above, and incubated with either ubiquitin conjugates (+) or buffer (-). Samples were resolved by native PAGE and visualized by suc-LLVY-AMC hydrolysis. While the incorporation of *rpn13-pru* into the *rpn10-uim* background attenuates the conjugate-induced electrophoretic mobility shift (compare lanes 2 and 6), deletion of *SEM1* shows no discernible effect.

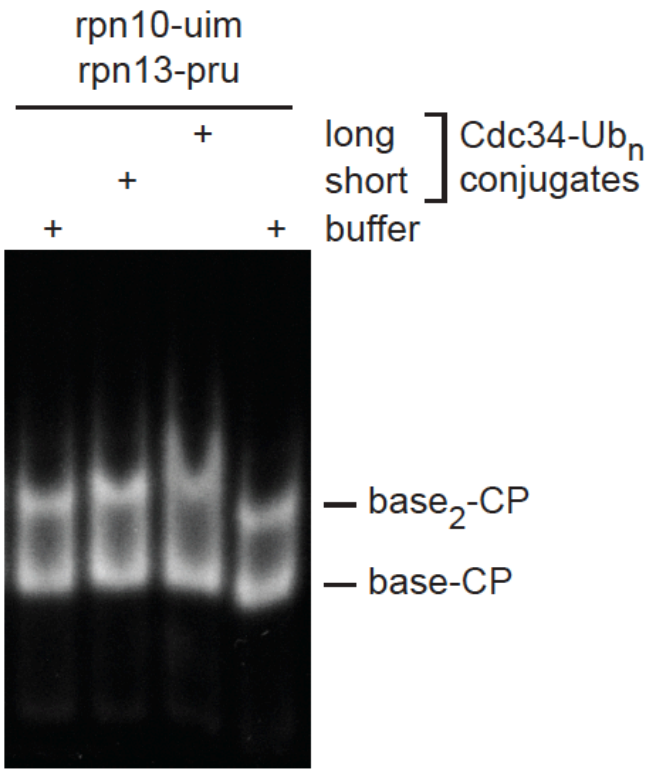

Fig. S3.

Evidence for ubiquitin receptors in addition to Rpn10 and Rpn13 in the base. Base purified from strains containing the mutations *rpn10-uim* and *rpn13-pru* was purified as described and reconstituted with CP to form base-CP complexes. Base-CP was incubated with Cdc34-ubiquitin conjugates and resolved via native PAGE and developed as described previously.

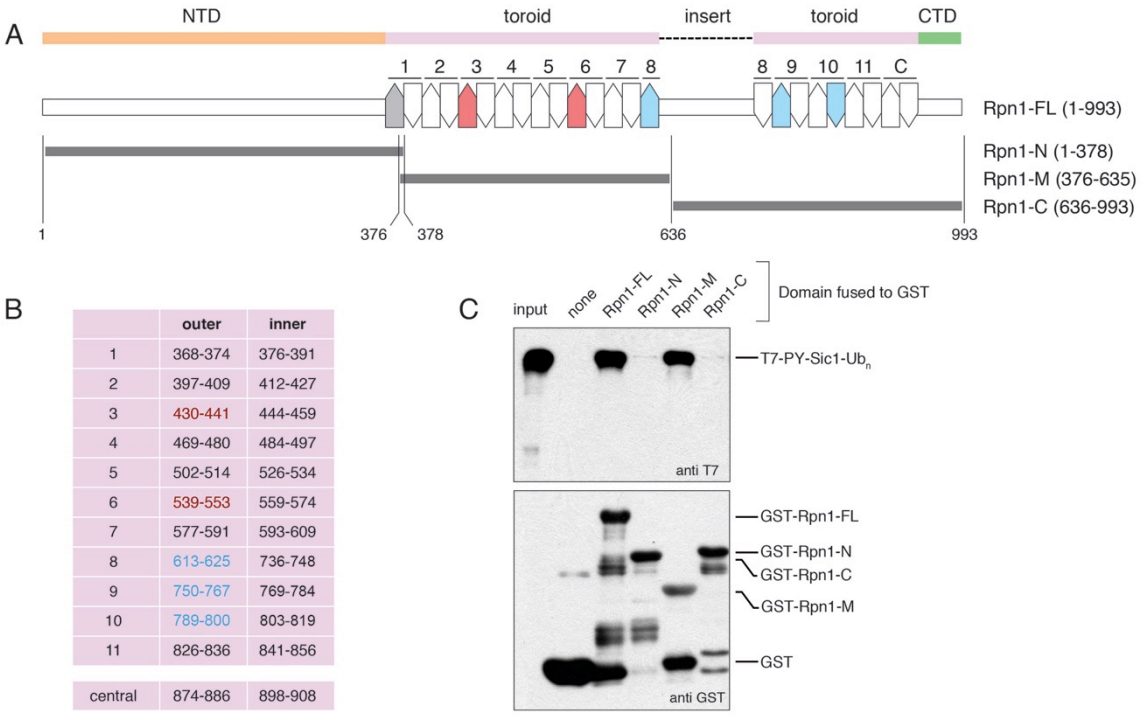

	outer	inner
1	368-374	376-391
2	397-409	412-427
3	430-441	444-459
4	469-480	484-497
5	502-514	526-534
6	539-553	559-574
7	577-591	593-609
8	613-625	736-748
9	750-767	769-784
10	789-800	803-819
11	826-836	841-856
central	874-886	898-908

Fig. S4.

Mapping of a ubiquitin binding site in Rpn1. **(A)** Schematic of Rpn1. The central toroid domain (purple) is flanked by an N-terminal domain (orange), and a C-terminal domain (green), and interrupted by a highly charged and presumably flexible loop (dotted line). The toroid is composed of a series of hairpins (numbered 1-11), each with an outer and inner helix, shown as upward and downward arrows, respectively. The first element of hairpin 1, rendered in grey, is an extended loop rather than an alpha helix. The inner helices pack against a central hairpin (labeled C). Regions of interest described in Figures 1-5 (outer helix 6) and Figure 6 (outer helix 3) are rendered in red. Outer helices that appear to form contacts with Rpt1 and Rpt2 are rendered in blue. This model is based on NMR data, cryo-EM data (*47*), analogy to the paralogous proteasome subunit Rpn2 (*19*), and prior modeling by Kajava (*20*); the crystal structure of Rpn1 has not been determined. **(B)** Endpoints of the toroidal elements, based on cryo-EM data (*47*). Residue ranges for each of the helices in the toroidal domain are indicated. Colored text indicates elements depicted in panel (A). **(C)** Ubiquitin conjugate binding assays were carried out as Figure 1C.

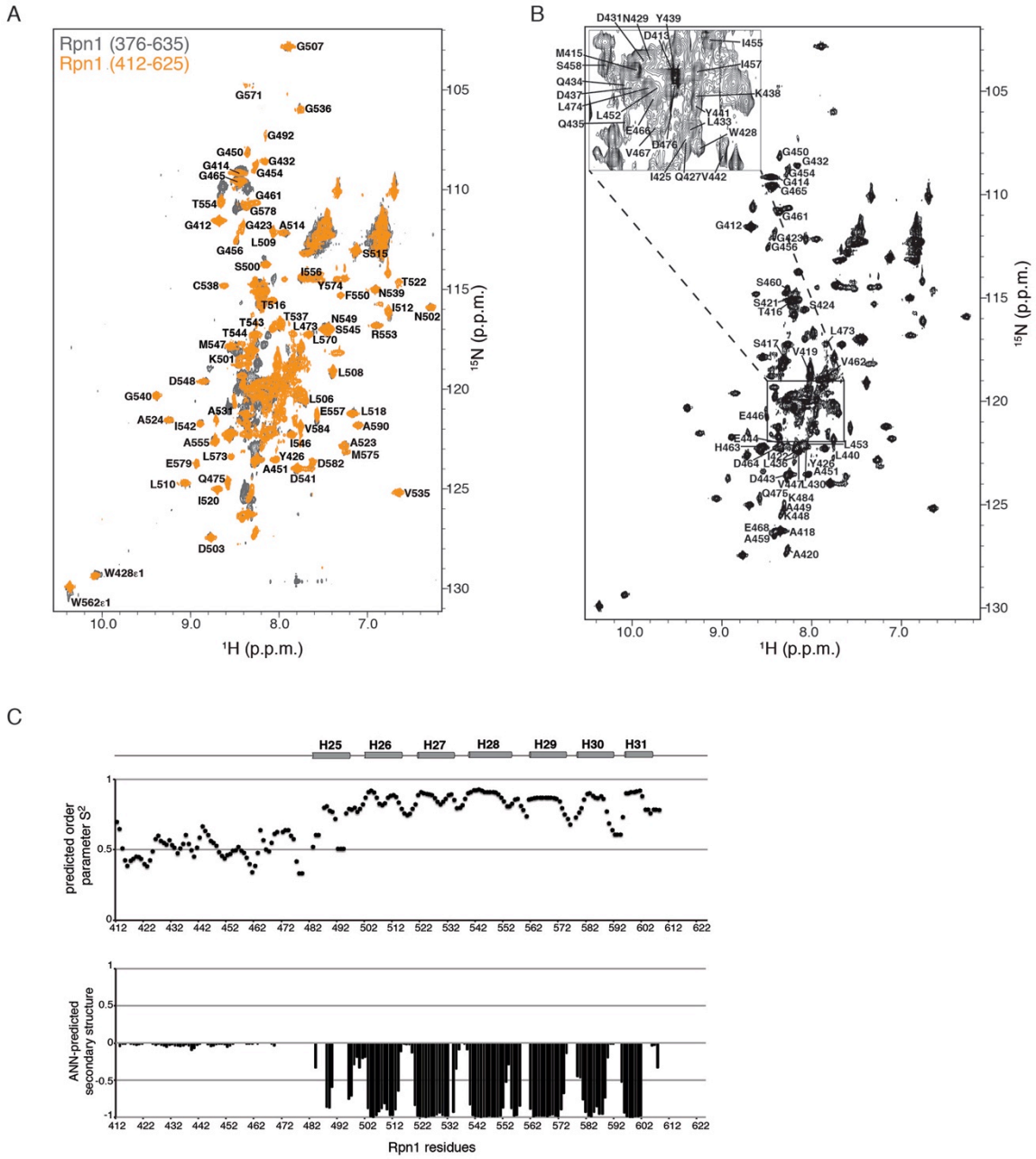

Fig. S5.

Chemical shift and secondary structure assignment of Rpn1$_{412\text{-}625}$. (A) Superimposed ^{1}H, ^{15}N HSQC spectra of ^{15}N Rpn1 fragments spanning 376-635 (grey) and 412-625 (orange). All dispersed signals have been assigned for Rpn1$_{412\text{-}625}$. **(B)** ^{1}H, ^{15}N HSQC spectra of ^{15}N Rpn1$_{412\text{-}625}$ with assignments for the disordered N-terminal portion displayed; these congest at regions characteristic of random coil. **(C)** Graphs of secondary structure (lower panel) and order parameters S2 (upper panel) calculated by TALOS+ from Rpn1$_{412\text{-}625}$ HN, Hα, Cα, Cβ, CO and N chemical shift assignments.

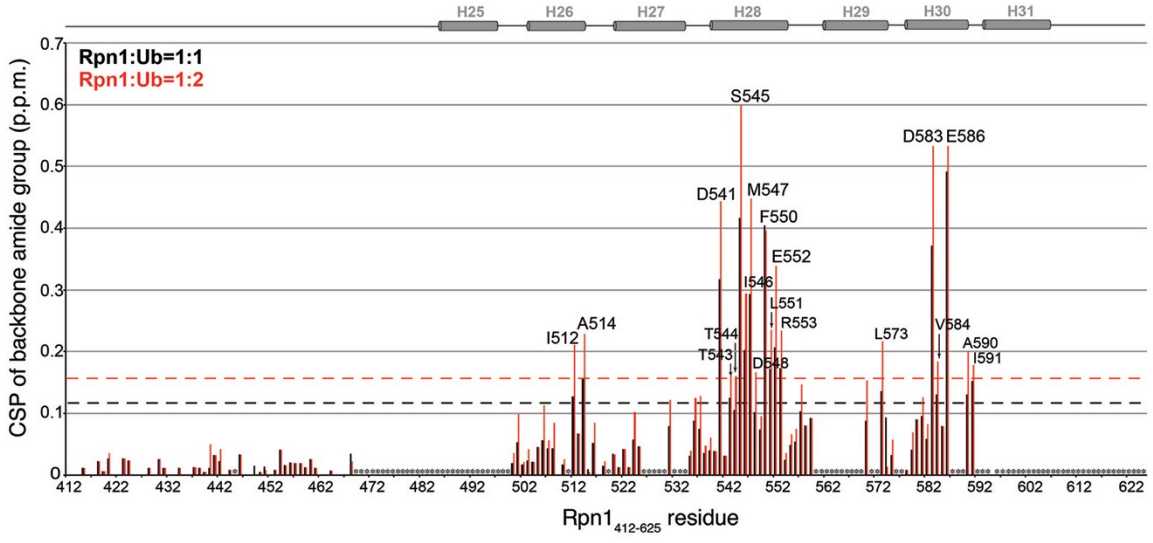

Fig. S6.

Identification of the ubiquitin-contact surface in the Rpn1 T1 site by using an NMR-based titration experiment. Amide signal shifting in ^{1}H, ^{15}N HSQC spectra for ^{15}N $Rpn1_{412\text{-}625}$ caused by addition of equimolar (black) or 2-fold molar excess (red) monoubiquitin. Designated helices as assigned in fig. S5 are included above the plot. Dotted lines indicates one standard deviation above average. Unassigned, overlapping, or proline groups are excluded from these analyses and indicated (*). CSP, chemical shift perturbation; p.p.m., part per million.

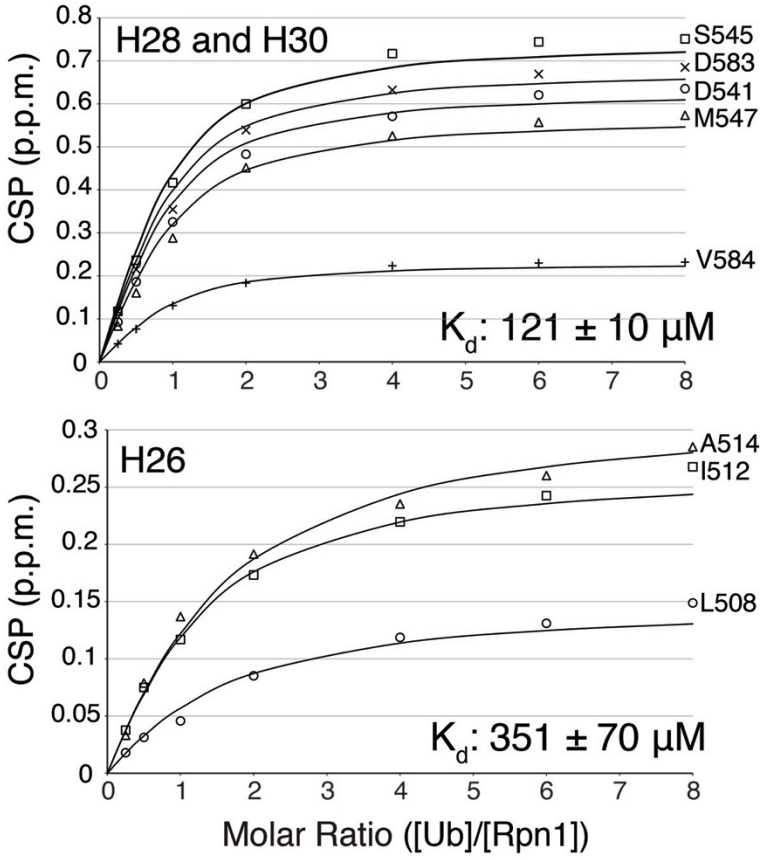

Fig. S7.

Two weak binding sites for monoubiquitin are identified from an NMR-based titration experiment. Shifting for indicated $Rpn1_{412\text{-}625}$ residues in Figure S6 is plotted with increasing ubiquitin:Rpn1 molar ratio and fit to the listed K_d values by using Microsoft Excel. CSP, chemical shift perturbation; p. p. m., part per million.

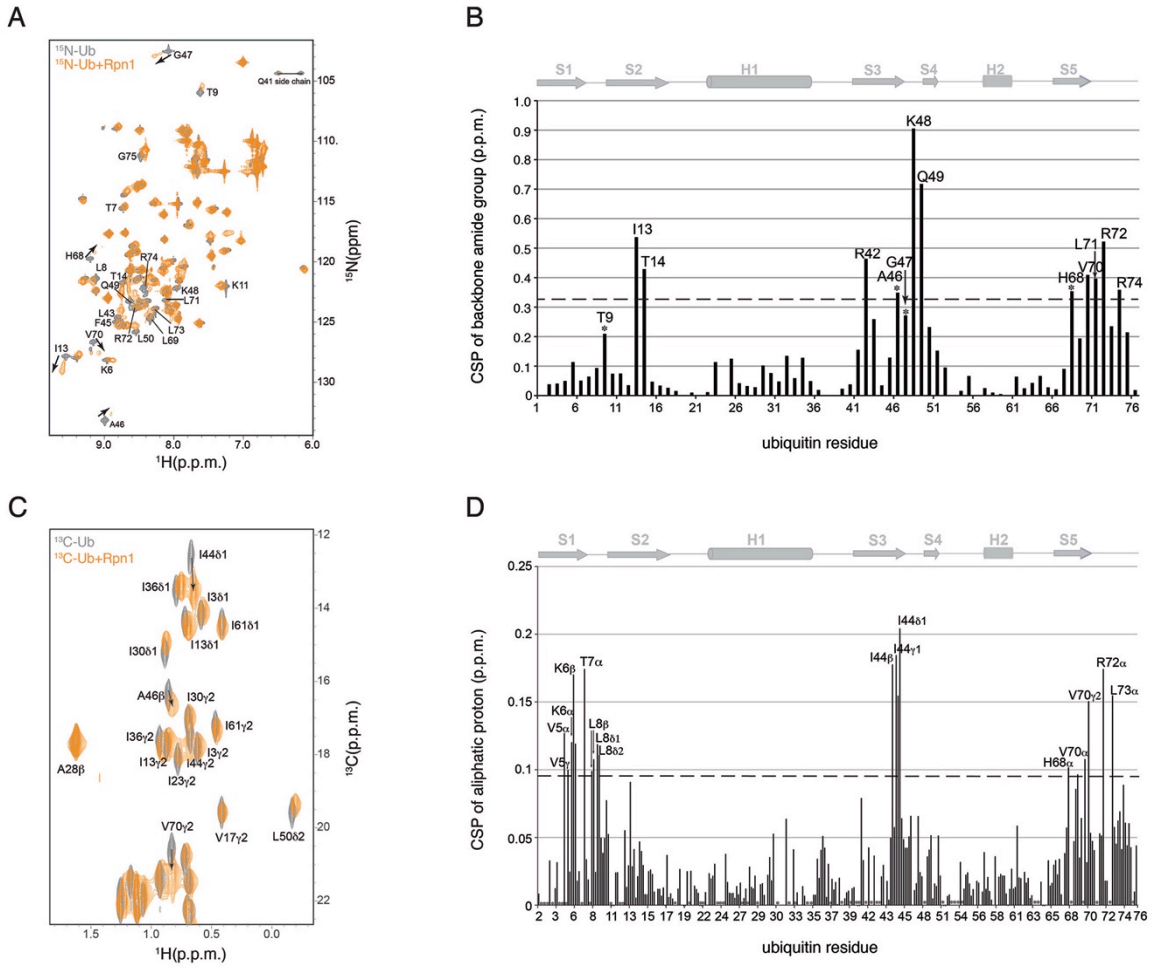

Fig. S8.

The Rpn1:ubiquitin interaction involves the hydrophobic patch of ubiquitin. (A) ^{1}H, ^{15}N HSQC spectra of ^{15}N ubiquitin (grey) and with (orange) equimolar $Rpn1_{412\text{-}625}$. **(B)** Signal shifting of ubiquitin amide groups upon addition of equimolar $Rpn1_{412\text{-}625}$ from (A) quantified and plotted. The dotted line in this figure and in (D) indicates one standard deviation above average. Secondary structure elements for ubiquitin are included above the plot. Resonances attenuated upon Rpn1 addition are indicated by an asterisk; these signals do not disappear but become weak. **(C)** Expanded region of ^{1}H, ^{13}C HSQC spectra of ^{13}C ubiquitin (grey) and with (orange) equimolar $Rpn1_{412\text{-}625}$. **(D)** Signal shifting of ubiquitin sidechain groups upon addition of equimolar $Rpn1_{412\text{-}625}$ from (C) is quantified and plotted. Overlapping groups excluded from this analysis are indicated by asterisks positioned just above the baseline. CSP, chemical shift perturbation; p. p. m., part per million.

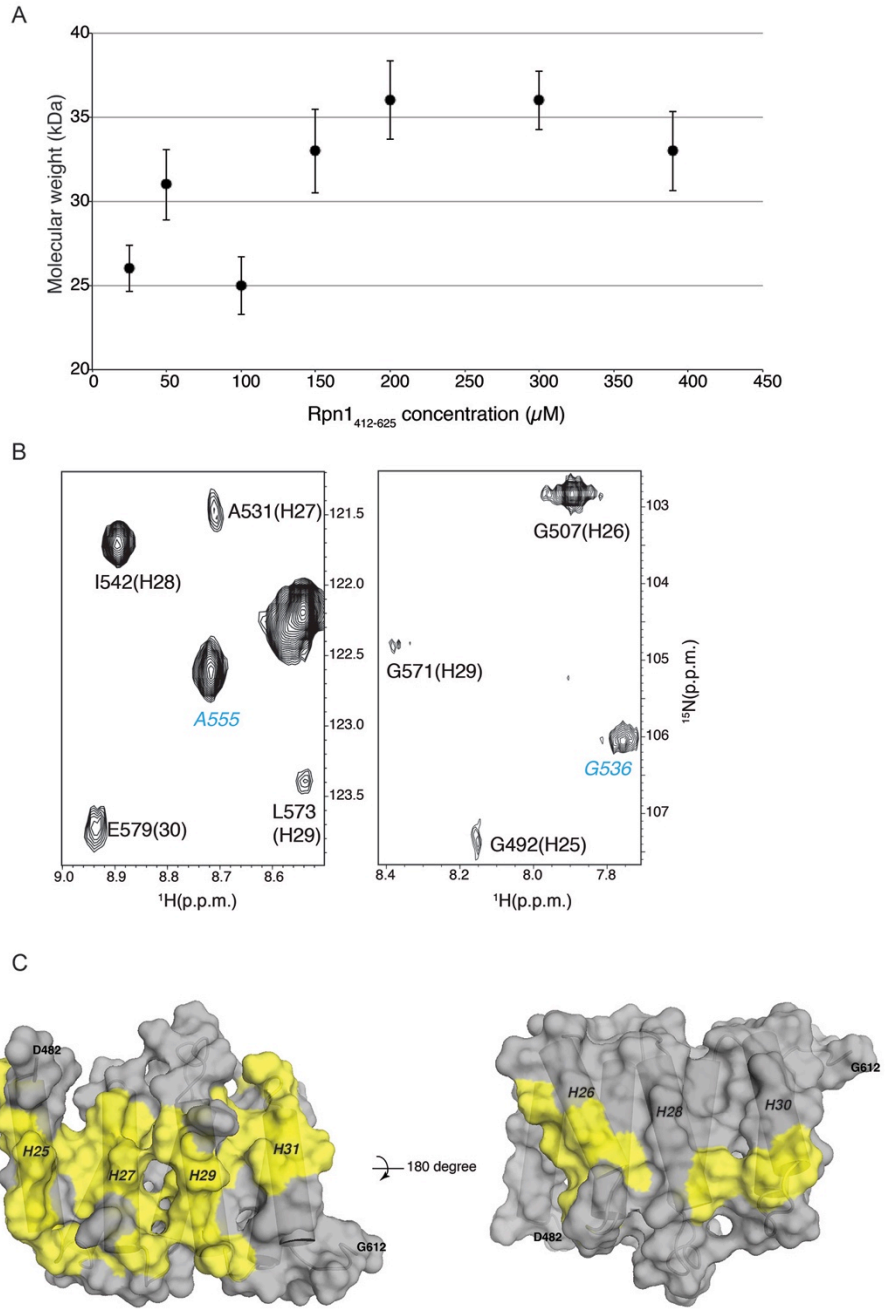

Fig. S9.

Rpn1$_{412-625}$ undergoes concentration-dependent dimerization, most likely mediated by the inner helices of the toroid. (A) Molecular weight of Rpn1$_{412-625}$ present at varying protein concentration, assessed by dynamic light scattering. **(B)** Expanded regions of a ^{15}N Rpn1$_{412-625}$ ^{1}H, ^{15}N HSQC spectrum with amide signals from residues in helices or loops labeled in black or blue, respectively. Signals from H25, H27, and H29 are attenuated compared to those from H26 and H28. **(C)** Rpn1$_{482-612}$ surface diagram with exposed hydrophobic regions colored yellow. The orientation of the two views is rotated by 180°.

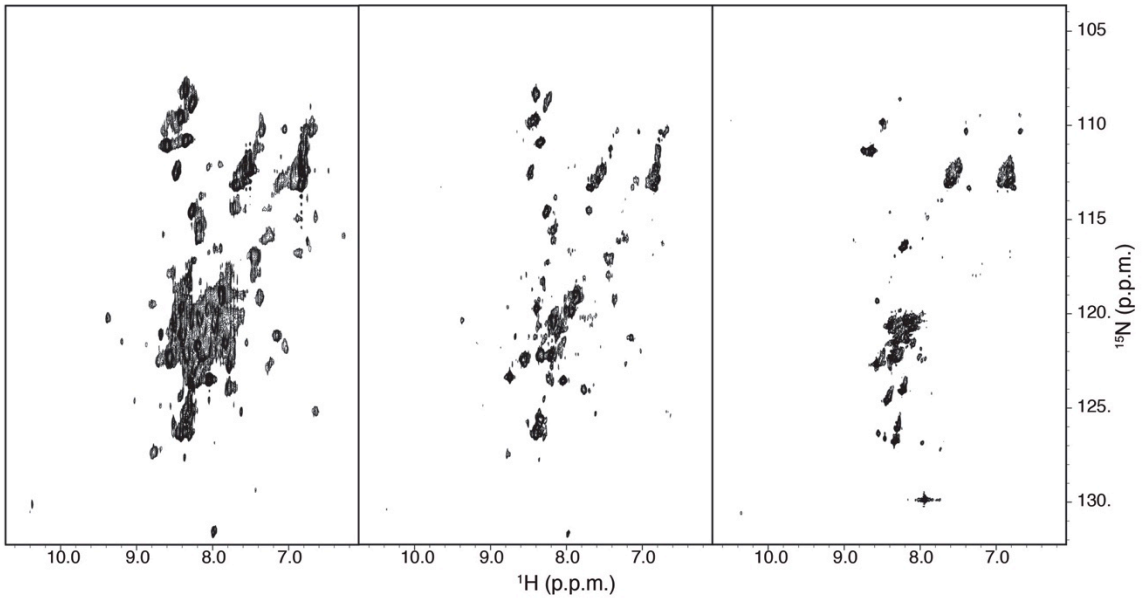

Fig. S10.

Deletions at the N- and C-terminal ends of Rpn1$_{412\text{-}625}$ destabilize the protein fold. ^{1}H, ^{15}N HSQC spectra of ^{15}N Rpn1 fragments spanning 432-625 (left), 446-625 (middle), and 465-592 (right). None of these spectra are of the quality displayed in fig. S5A for Rpn1$_{412\text{-}625}$.

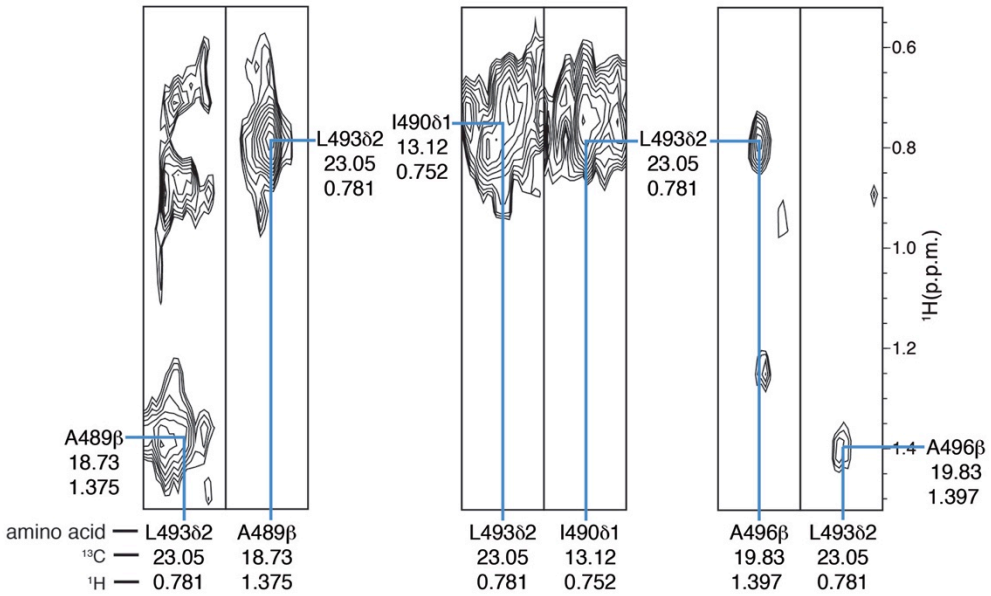

Fig. S11.

NOE interactions between methyl groups were critical to resolving the structure of the Rpn1 T1 site. Unambiguous NOE assignments involving methyl groups were made by using 4D methyl-methyl HMQC-NOESY-HMQC experiments with 200 ms mixing times recorded on ^{2}H, ^{15}N, $^{13}C^{1}H_3$ -methyl (Ileδ1, Leu, Val) labeled $Rpn1_{412\text{-}625}$ (not displayed) or ^{2}H, ^{15}N, $^{13}C^{1}H_3$ -methyl (Ileδ1, Ala, Met), Leu/Val $^{13}C^{1}H_3^{proS}$ labeled $Rpn1_{412\text{-}625}$. Selected regions from the spectrum recorded on the latter sample display NOE interactions between methyl protons of A489 and L493, I490 and L493, and L493 and A496; these define Rpn1 H25. All values are given in parts per million (ppm) units.

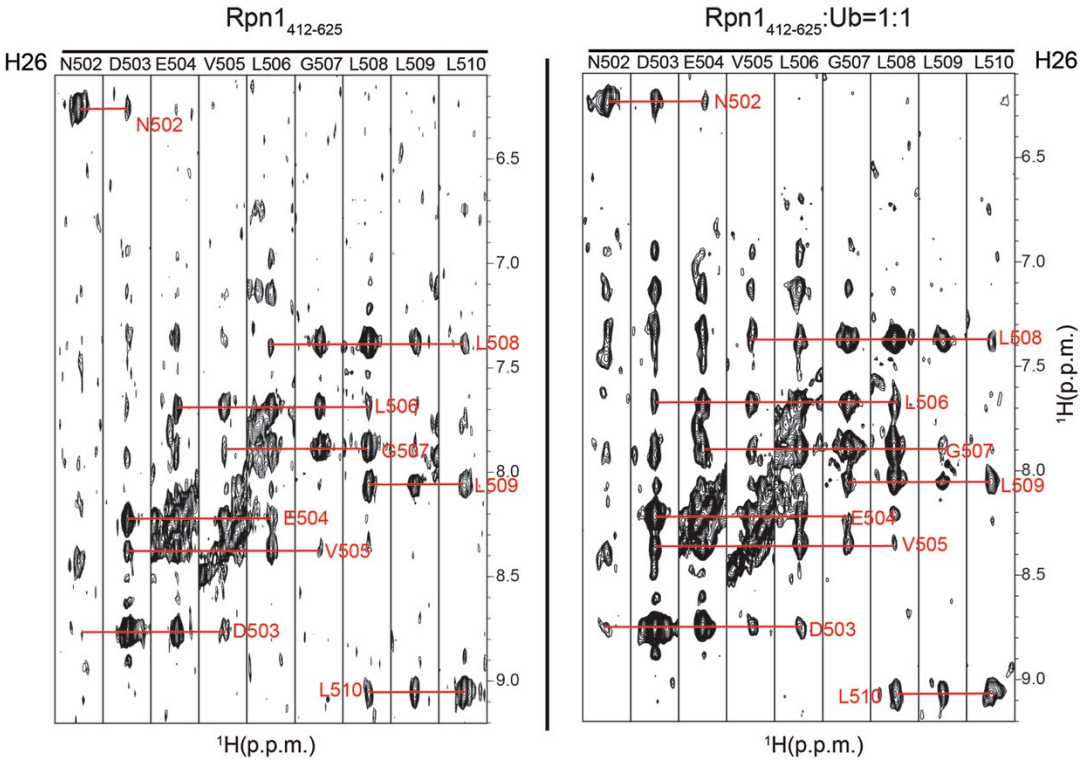

Fig. S12.

Amide-amide NOE interactions for H26 of the Rpn1 T1 site in its free and ubiquitin-bound state demonstrating an increased signal-to-noise ratio for the complex. The NOE patterns observed in ^{15}N dispersed NOESY spectra recorded on ^{15}N-labeled Rpn1$_{412-625}$ (left) or the ^{15}N-labeled Rpn1$_{412-625}$:ubiquitin complex (right). All sample and acquisition parameters are identical; a mixing time of 200 ms was used and 900 MHz spectrometer equipped with a cryogenically cooled probe.

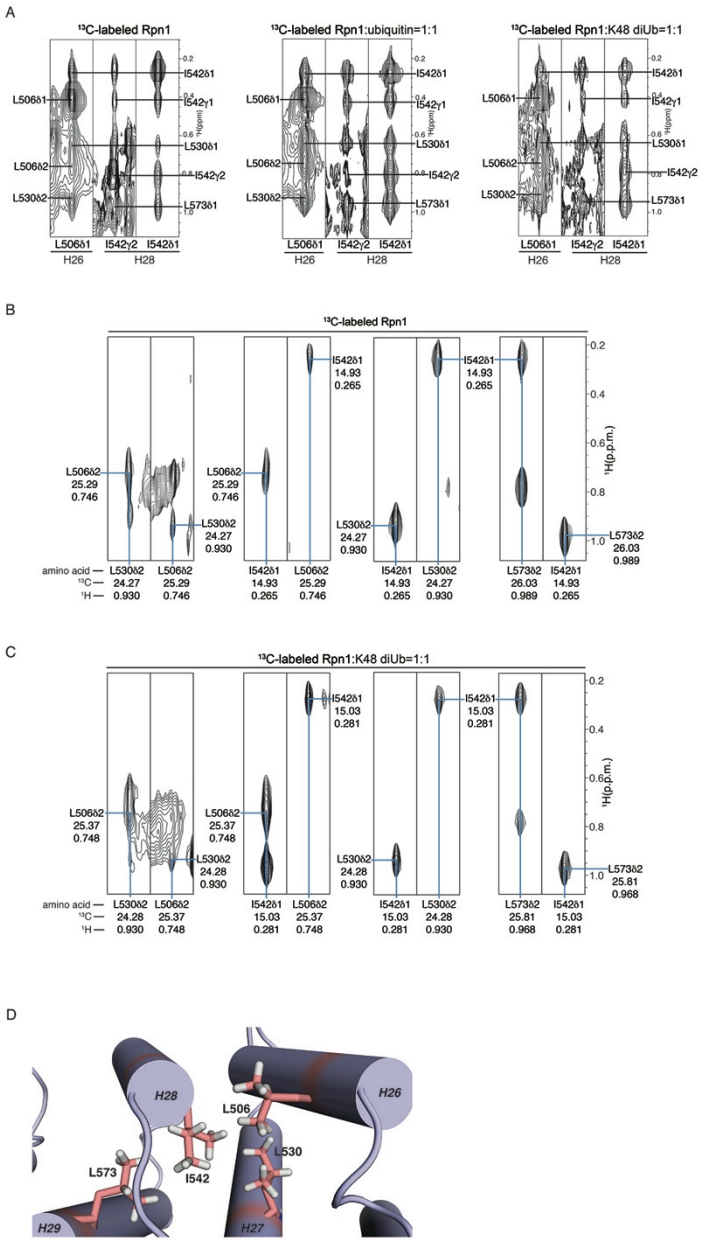

Fig. S13.

The Rpn1 T1 site structure does not change upon binding to ubiquitin or K48-linked diubiquitin. (A) Selected regions from a ^{1}H, ^{13}C dispersed NOESY experiments acquired with ^{13}C-labeled $Rpn1_{412-625}$ free (left), ^{13}C-labeled $Rpn1_{412-625}$ mixed with equimolar unlabeled ubiquitin (middle) or ^{13}C-labeled $Rpn1_{412-625}$ mixed with equimolar unlabeled K48-linked diubiquitin (right) highlighting inter-residue NOE interactions between L506 (H26), L530 (H27), I542 (H28) and L573 (H29), which are displayed in a ribbon diagram of $Rpn1_{482-612}$ (D). (B, C) Selected regions from 4D methyl-methyl HMQC-NOESY-HMQC experiments acquired with ^{2}H, ^{15}N, $^{13}C^{1}H_3$ -methyl (Ileδ1, Ala, Met), Leu/Val $^{13}C^{1}H_3^{proS}$ labeled $Rpn1_{412-625}$ free (B) or ^{2}H, ^{15}N, $^{13}C^{1}H_3$ -methyl (Ileδ1, Leu, Val) labeled $Rpn1_{412-625}$ mixed with equimolar unlabeled K48-linked

diubiquitin (C), illustrating NOE interactions between methyl protons of L506 (H26), L530 (H27), I542 (H28) and L573 (H29). All values are given in parts per million (ppm) units.

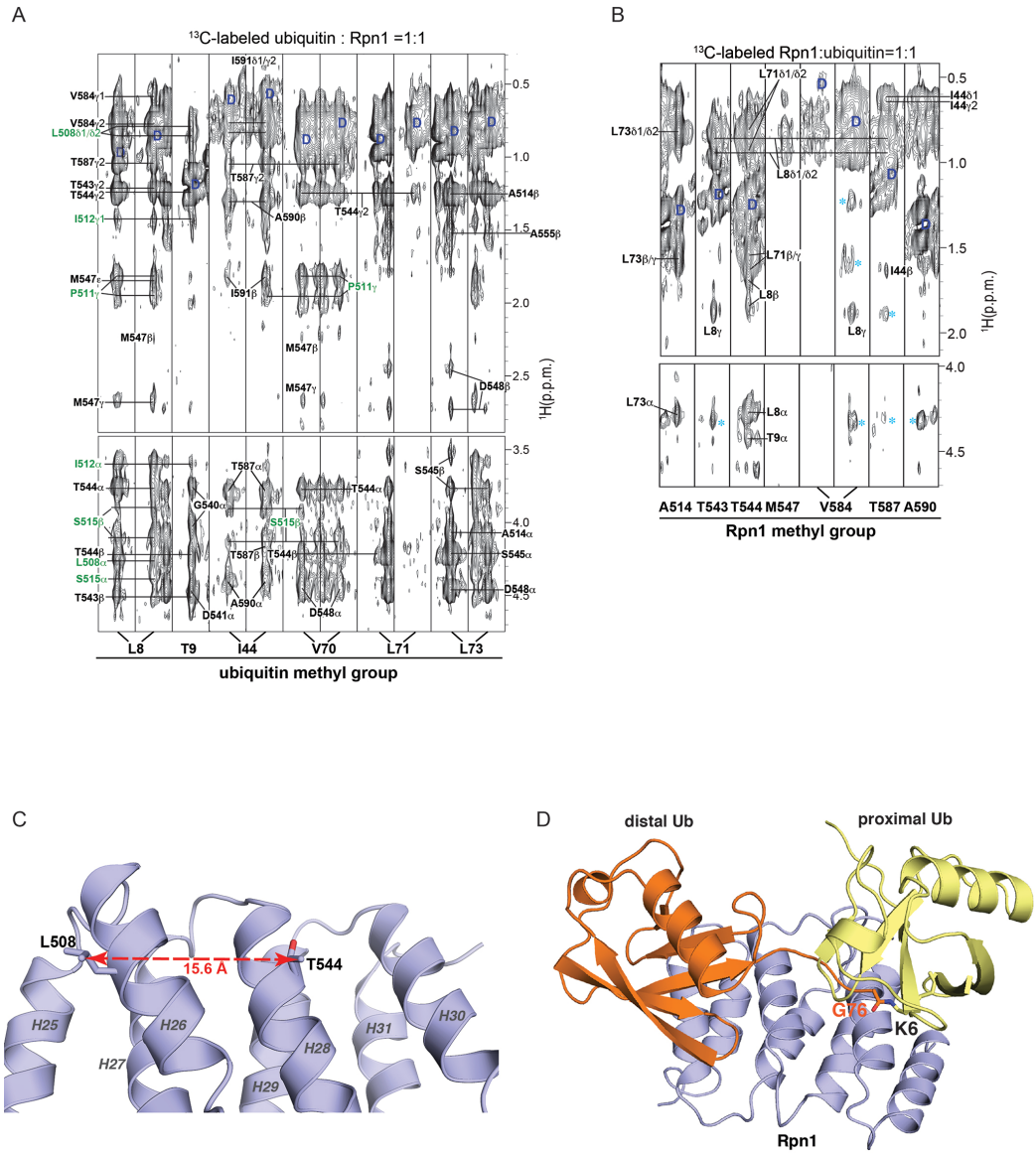

Fig. S14.

Intermolecular NOEs reflect the presence of two ubiquitin-binding surfaces on the Rpn1 T1 site. (A, B) Selected regions from a ^{1}H, ^{13}C half-filtered NOESY experiment acquired with ^{13}C-labeled ubiquitin and equimolar unlabeled $Rpn1_{412\text{-}625}$ (A) or ^{13}C-labeled $Rpn1_{412\text{-}625}$ and equimolar unlabeled ubiquitin (B) highlighting intermolecular NOE interactions. Breakthrough diagonal peaks are labeled (blue 'D'). Two sets of observed NOE interactions between Rpn1 and ubiquitin are distinguished with black and green labels. Signals that were also observed in a control ^{13}C-half-filtered 3D NOESY spectrum acquired on free ^{13}C-labeled $Rpn1_{412\text{-}625}$ are labeled (light blue asterisks); these are breakthrough peaks and not from intermolecular interactions. **(C)** Ribbon diagram of the Rpn1 T1 site illustrating the distance between the methyl groups of L508 and T544 in

red. **(D)** Model structure of the Rpn1 T1 site (blue) complexed with K6-linked diubiquitin (orange and yellow) formed by linking G76 from the ubiquitin at H28/H30 to the K6 sidechain from the ubiquitin at H26 for the structure displayed in Fig 2B. The model structure was energy minimized by using Schrodinger.

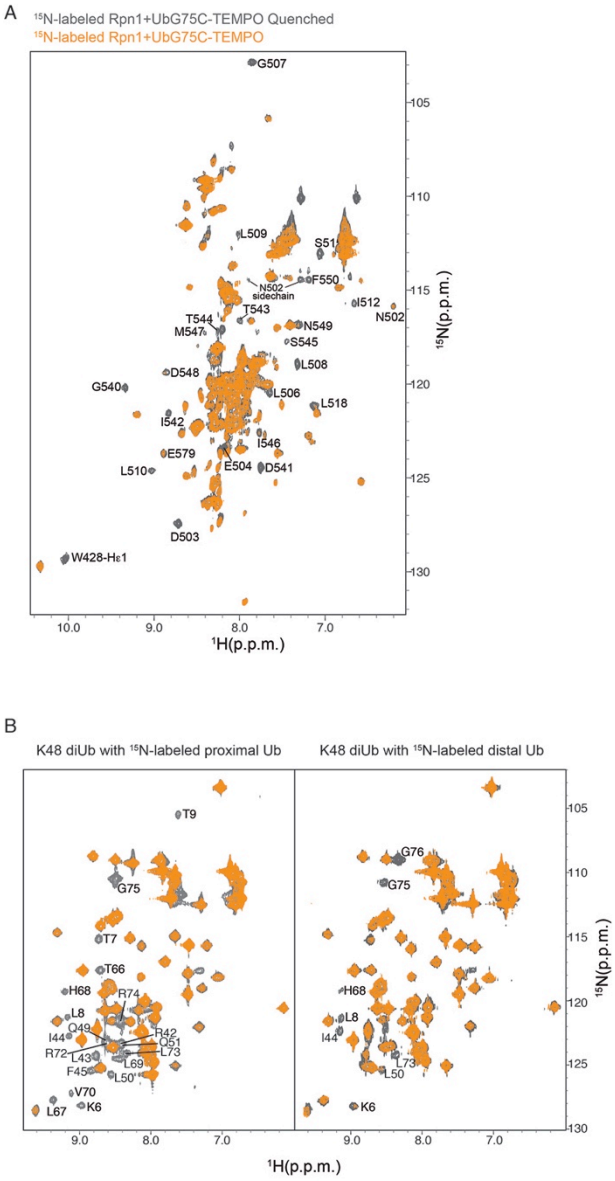

Fig. S15.

Spin labeling experiments report on the Rpn1 T1 interaction with ubiquitin and K48-linked diubiquitin. (A) ^{1}H, ^{15}N HSQC spectrum of 0.3 mM ^{15}N-labeled Rpn1$_{412\text{-}625}$ mixed with equimolar ubiquitin in which G75 is replaced with cysteine and adducted to the spin label TEMPO (orange), and following quenching by 5 mM ascorbic acid (grey). Rpn1 signals attenuated by the spin label are labeled. **(B)** ^{1}H, ^{15}N HSQC spectrum of 0.3 mM K48-linked diubiquitin with ^{15}N-labeling at either the proximal (left panel) or distal (right panel) ubiquitin and mixed with equimolar Rpn1$_{412\text{-}625}$ (L518C, C538A, C606A) spin labeled with MTSL (orange), and following quenching by 5 mM ascorbic acid (grey). Ubiquitin signals attenuated by the spin label on Rpn1 are labeled.

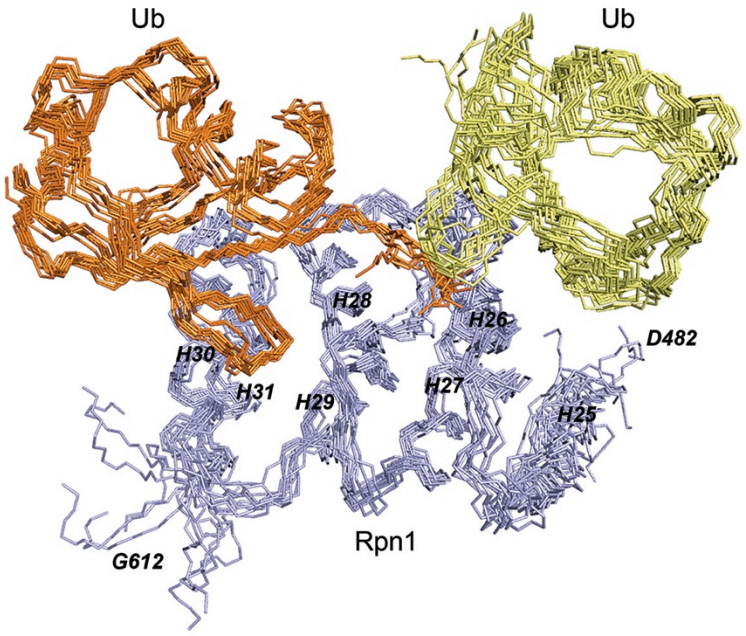

Fig. S16.

Structure of the Rpn1 T1:monoubiquitin complex. Backbone trace for the ten lowest energy Rpn1 T1:ubiquitin structures from 50 linear starting structures superimposed by secondary structure elements of ubiquitin and $Rpn1_{482-612}$. Rpn1 T1, blue; ubiquitin, orange and yellow. These structures were calculated by using the constraints summarized in Table S2. Briefly, intermolecular distance constraints determined by ^{13}C-half-filtered 3D NOESY experiments on samples of ^{13}C-labeled monoubiquitin:unlabeled $Rpn1_{412-625}$ and ^{13}C-labeled $Rpn1_{412-625}$:unlabeled monoubiquitin were used, as well as intramolecular restraints for $Rpn1_{482-612}$ as determined from $^{15}N/^{13}C$ NOESY spectra acquired on $^{15}N/^{13}C$-labeled $Rpn1_{412-625}$:monoubiquitin. PRE-derived intermolecular distance constraints were also used. Published constraints for free ubiquitin (PDB: 1D3Z) were used, as the ubiquitin structure does not change upon complex formation.

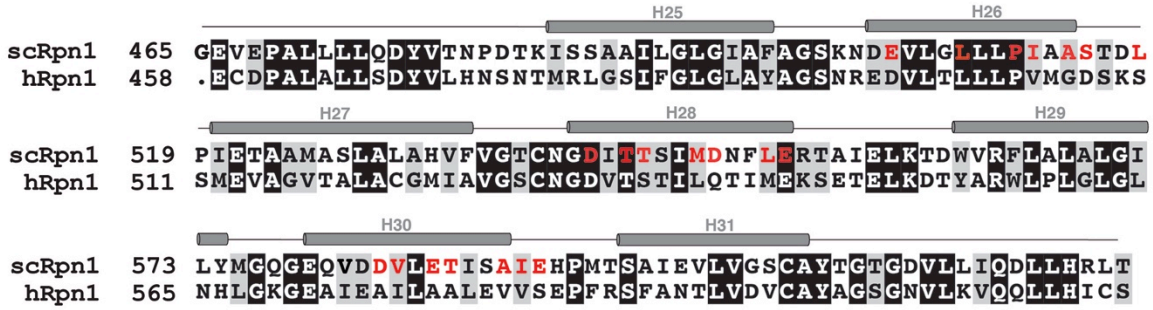

Fig. S17.

Many amino acids involved in binding to ubiquitin and Rad23 are conserved between human and yeast Rpn1. Rpn1 sequence alignment from *Saccharomyces cerevisiae* and *homo sapiens* shading identical (black) and conserved (grey) residues, and indicating those that interact with ubiquitin in red. Secondary structure assignments as determined by NMR are included above the sequence.

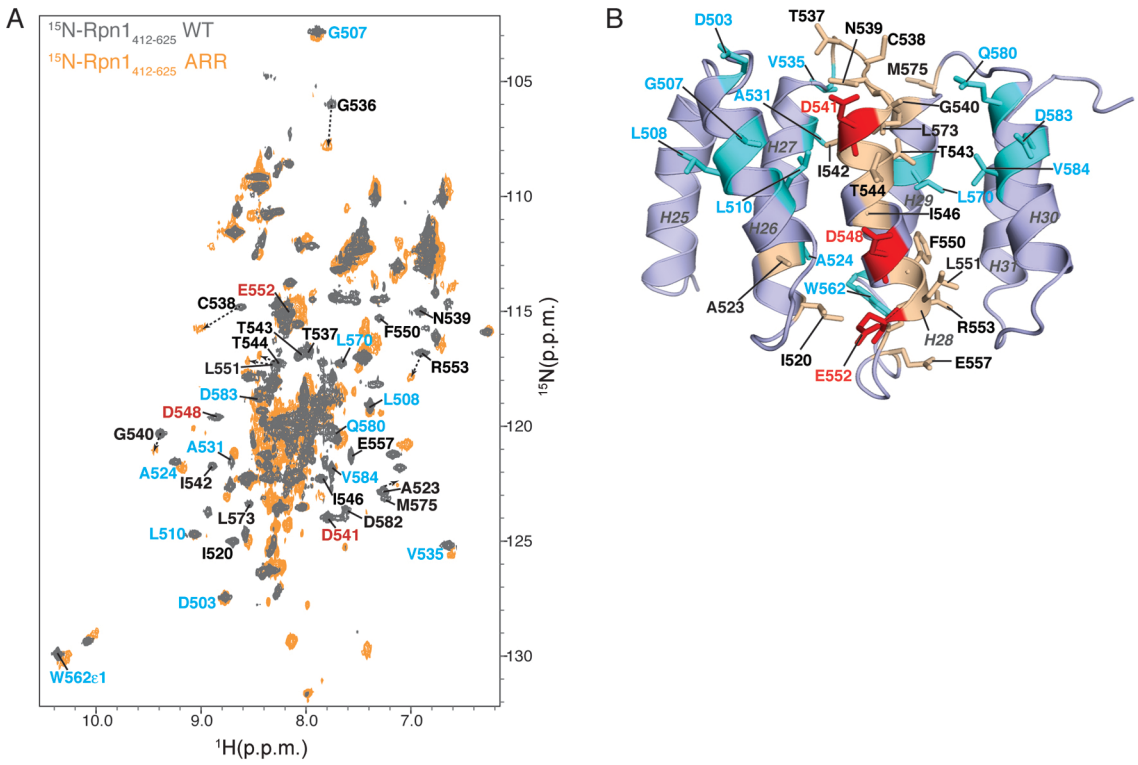

Fig. S18.

The structural integrity of the Rpn1 toroid is maintained in the Rpn1-ARR mutant. (A) ^{1}H, ^{15}N HSQC spectra of 0.4 mM ^{15}N Rpn1$_{412\text{-}625}$ (grey) superimposed with 0.2 mM ^{15}N Rpn1$_{412\text{-}625}$ with D541A, D548R, and E552R substitutions (Rpn1-ARR, orange). Signals from D541, D548, and E552 in the Rpn1 T1 WT spectrum are labeled in red; these are as expected missing from the Rpn1 T1 ARR spectrum. Signals from amino acids that are spatially close to D541, D548, or E552 also shift in some cases and these are labeled in black; dashed arrows are used to indicate likely positions in the Rpn1-ARR spectrum. Signals from amino acids in H26, H27, H29 and H30 that are unchanged by the D541A, D548R, and E552R substitutions are labeled in blue; these unperturbed signals throughout the T1 region indicate that its overall structure is maintained. (B) Ribbon diagram of the Rpn1 T1 site with D541, D548, and E552 illustrated in red and their neighboring amino acids, which show shifting in (A), displayed in beige. Various amino acids located in H26, H27, H29 and H30 that are unaffected by the D541A, D548R, and E552R substitutions are displayed in blue.

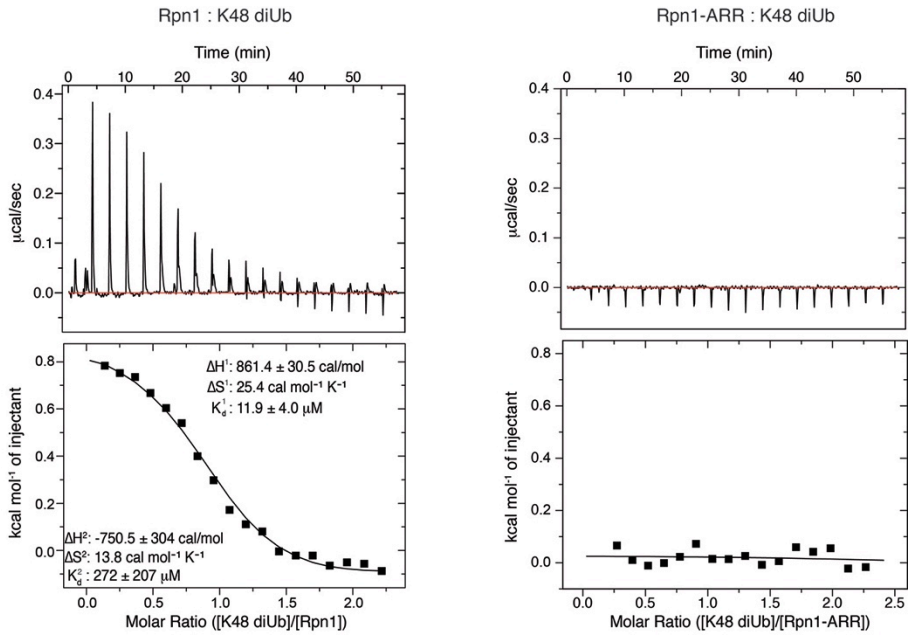

Fig. S19.

ITC measurements indicate lost binding to K48 diubiquitin at the Rpn1 T1 site following D541A D548R E552R mutations. ITC analysis of $Rpn1_{412-625}$ D541A D548R E552R (ARR, right) or wild-type (left) binding to K48 diubiquitin. The binding isotherms (top) were integrated to give the enthalpy change as a function of the molar ratio of K48 diubiquitin to Rpn1 (left, bottom) or Rpn1-ARR (right, bottom).

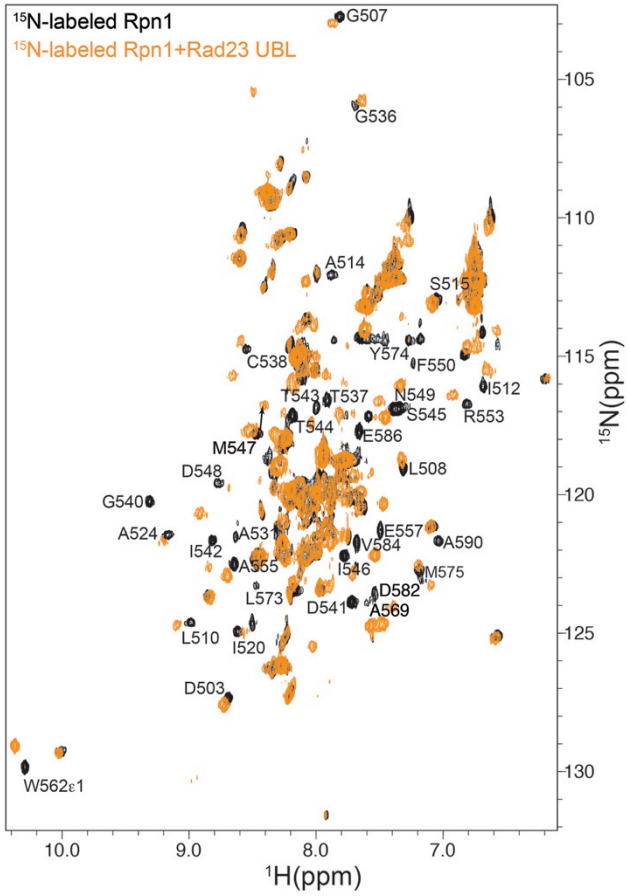

Fig. S20.

Mapping of the Rpn1 T1 residues involved in binding to the Rad23^{UBL} domain. ^{1}H, ^{15}N HSQC spectra of ^{15}N Rpn1$_{412-625}$ (black) and with equimolar Rad23^{UBL} (orange). Rpn1 signals that shift away from their unligated state following the addition of Rad23^{UBL} domain are labeled.

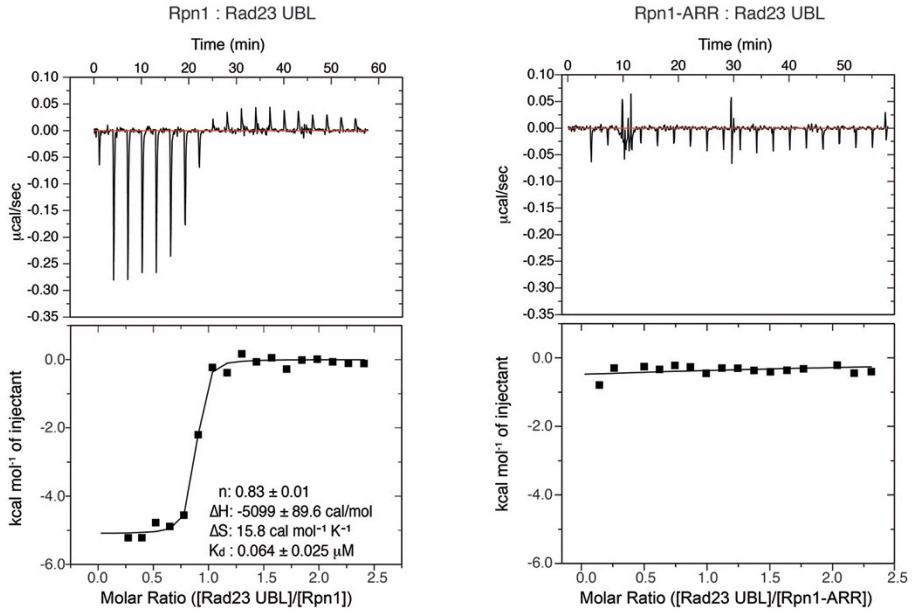

Fig. S21.

ITC measurements indicate lost binding to the Rad23^{UBL} domain following incorporation of the D541A D548R E552R mutations into the Rpn1 T1 site. ITC analysis of Rpn1$_{412-625}$ D541A D548R E552R (ARR, right) or wild-type (left) binding to the Rad23^{UBL} domain. The binding isotherms (top) were integrated to give the enthalpy change as a function of the molar ratio of Rad23^{UBL} domain to Rpn1 (left, bottom) or Rpn1-ARR (right, bottom).

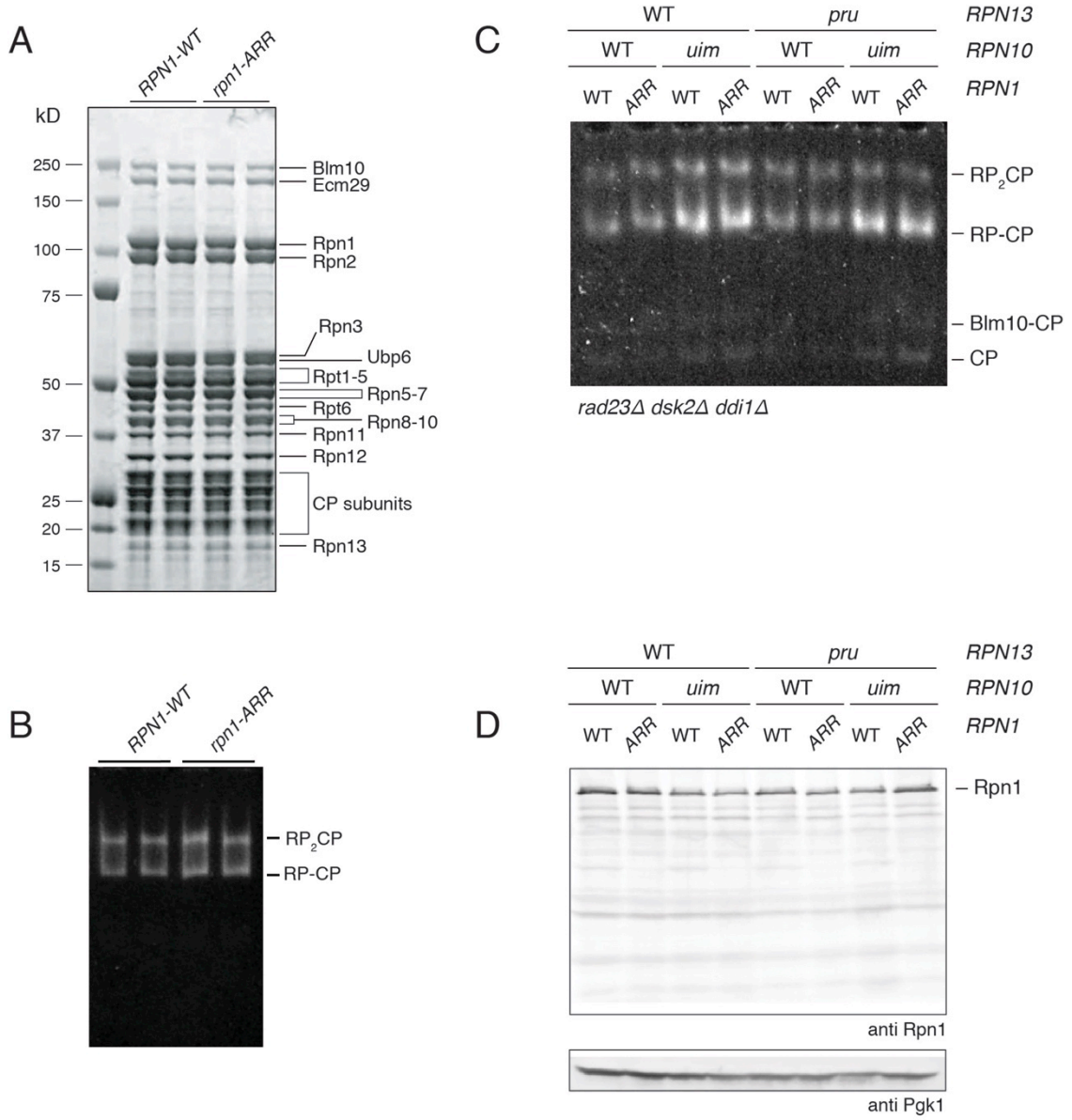

Fig. S22.

Rpn1-ARR proteasomes show no evident defects in composition, assembly, or in vivo abundance. (A) Proteasomes were purified in duplicate samples from strains with the background *rpn10-uim rpn13-pru rad23Δ dsk2Δ ddi1Δ*, resolved on SDS-PAGE, and stained with Coomassie Blue. **(B)** The same proteasome samples as shown in panel (A) were resolved via native PAGE, and active species were visualized with suc-LLVY-AMC as previously described. **(C)** Extracts of *rad23Δ dsk2Δ ddi1Δ* strains with the indicated additional mutations were prepared, and samples were directly resolved on native PAGE, with active proteasome species visualized by suc-LLVY-AMC hydrolysis. **(D)** The same extracts as shown in panel (C) were resolved by SDS-PAGE, blotted, and probed for Rpn1.

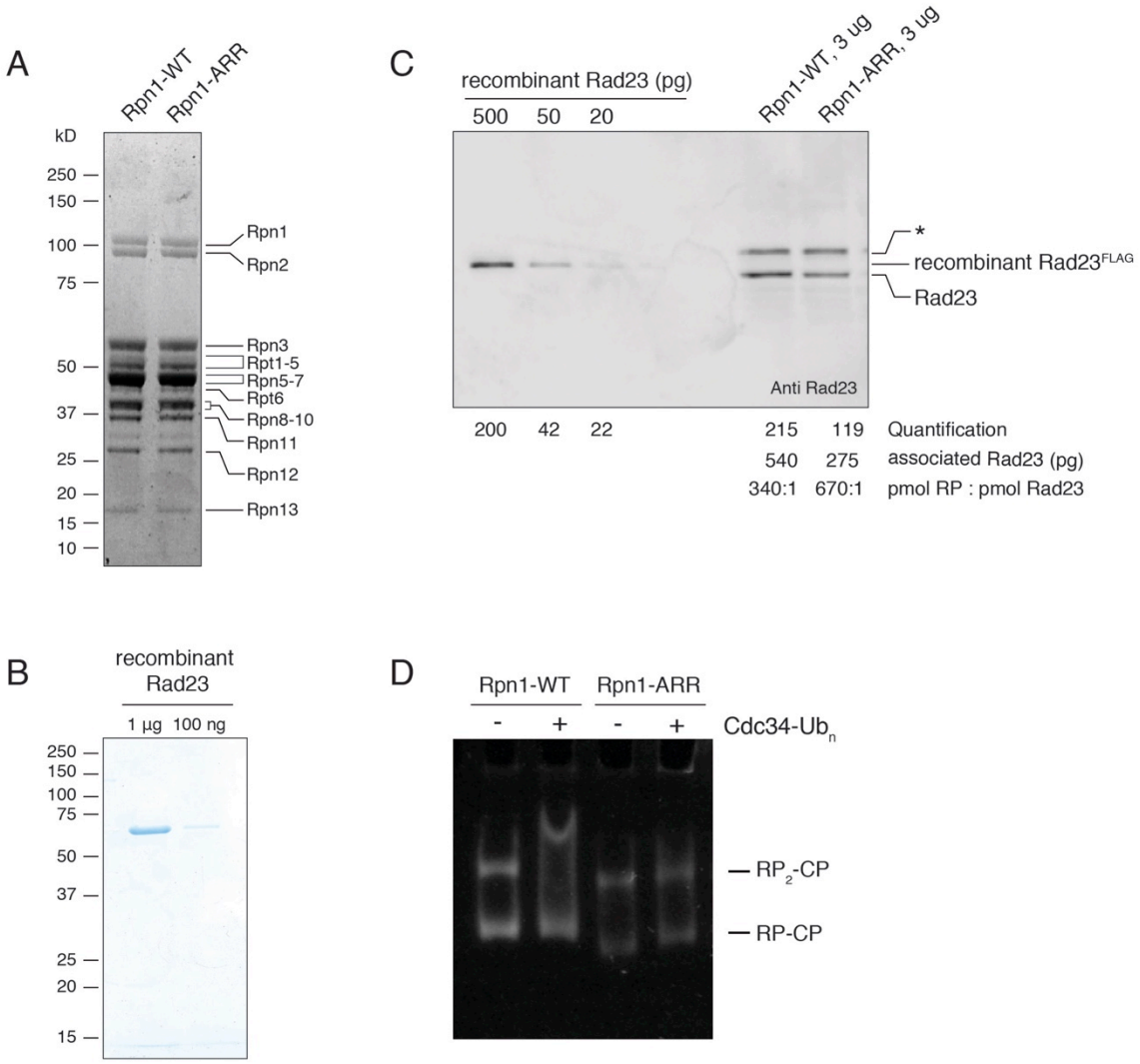

Fig. S23.

Residual Rad23 cannot account for the ubiquitin-binding deficit of the Rpn1-ARR proteasomes. (A) Regulatory particle with the indicated variations in Rpn1 was purified as described, and 3 µg was resolved by SDS-PAGE and stained with Coomassie blue. **(B)** Recombinant Rad23 was purified, resolved by SDS-PAGE, and stained with Coomassie blue. **(C)** Purified regulatory particles (from A) and purified recombinant Rad23 (from B) were resolved via SDS-PAGE, blotted, and probed with antibody to Rad23. Signals were quantified as described. The asterisk denotes a nonspecific cross-reactive band. **(D)** Regulatory particles were purified from *rpn10-uim rpn13-pru rad23Δ dsk2Δ ddi1Δ* strains, and incubated with core particle. Reconstituted proteasomes were incubated with ubiquitin conjugates or buffer and resolved via native PAGE. Active proteasome species were visualized by suc-LLVY-AMC hydrolysis.

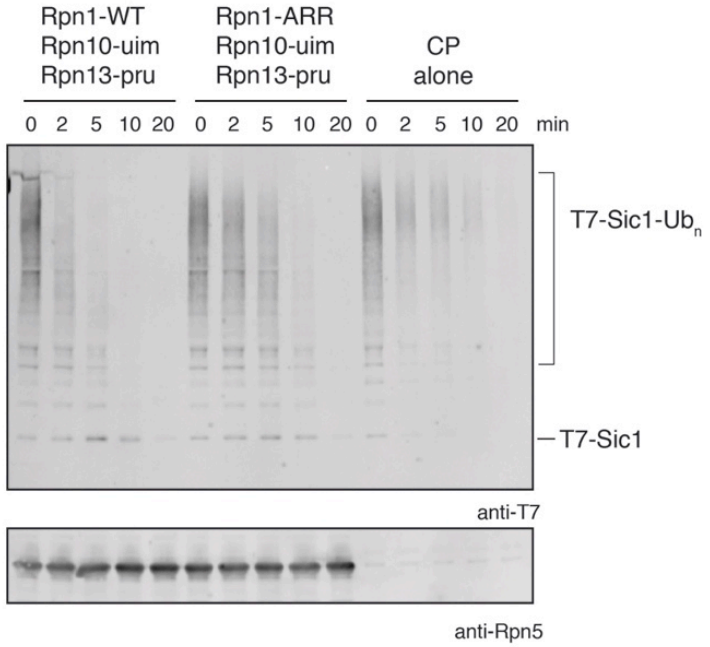

Fig. S24.

Rpn1 targets ubiquitinated PY-Sic1 to the proteasome for degradation. Purified RP from the indicated yeast strains was reconstituted with purified CP, and the resulting proteasomes were assayed for degradation of ubiquitinated PY-Sic1. Rpn5, an RP subunit, was probed as loading control. Based on the results with CP alone, it is likely that a component of the residual PY-Sic1 degradation seen with *rpn1-ARR rpn10-uim rpn13-pru* proteasomes is RP-independent and ubiquitin-independent.

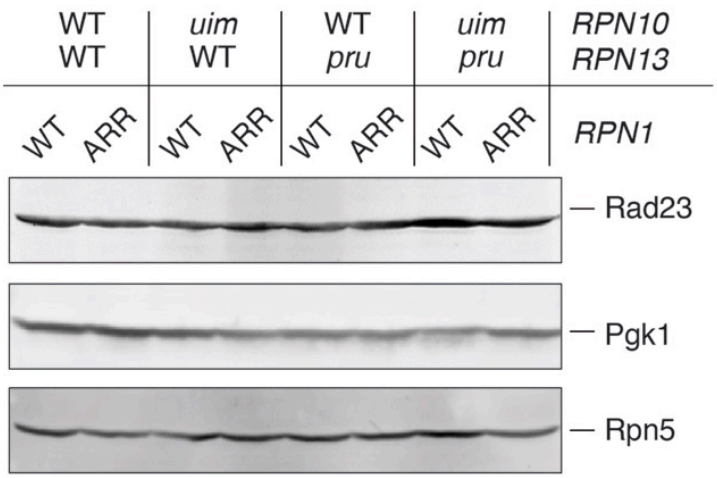

Fig. S25.

Mutations in intrinsic proteasomal ubiquitin receptors do not affect cellular levels of the proteasomal shuttling receptor Rad23. This experiment is a control for Figure 4E and other phenotypic studies. Extracts were prepared from yeast strains bearing the indicated mutations in genes encoding intrinsic ubiquitin receptors. Lysates were resolved by SDS-PAGE, blotted, and probed with antibodies to proteasome-associated UBL protein Rad23. Proteasome subunit Rpn5 and Pgk1 were probed as loading controls.

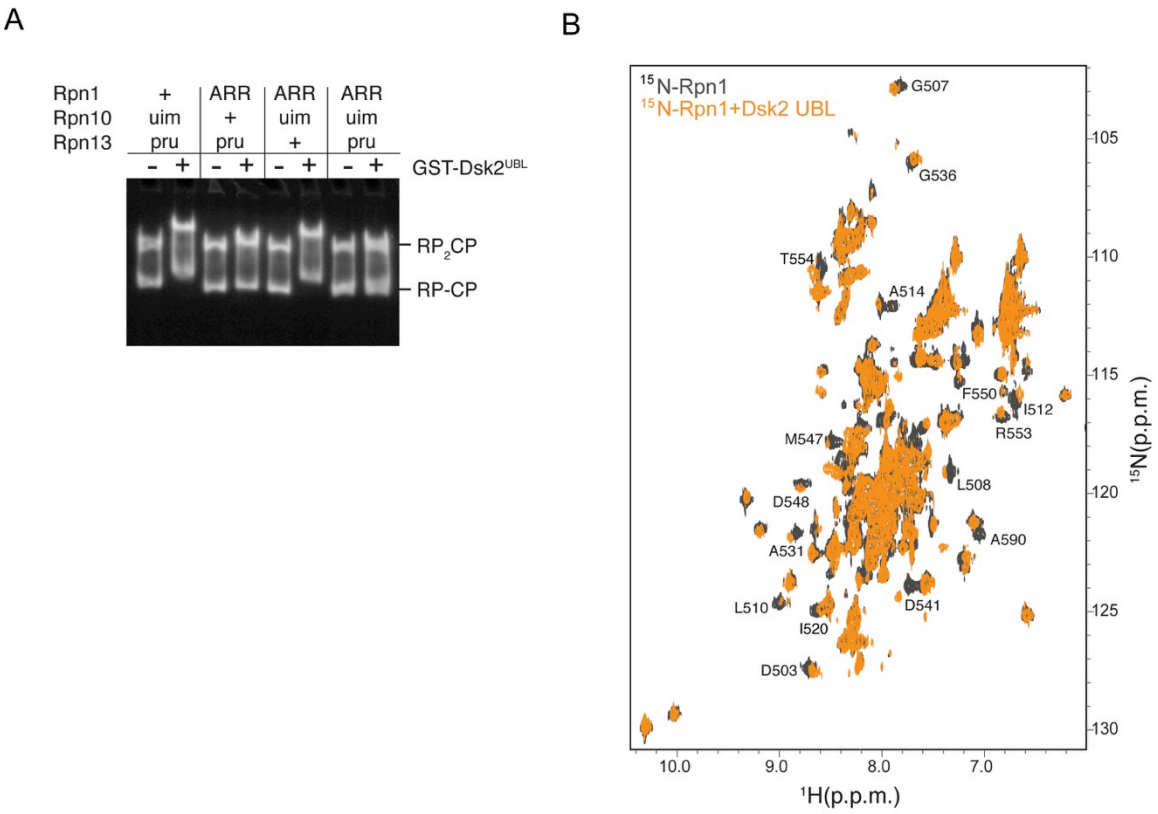

Fig. S26.

The Rpn1 T1 site binds the recombinant UBL domain of Dsk2. (A) Proteasome association with Dsk2^{UBL} evaluated by mobility shift assay. Proteasomes were purified from *rad23Δ dsk2Δ ddi1Δ* yeast strains bearing the indicated intrinsic ubiquitin receptor mutations, and incubated with GST-Dsk2^{UBL} at 100-fold molar excess. Complexes that include GST-Dsk2^{UBL} were resolved by native PAGE, and visualized using LLYV-AMC. The Dsk2 shift seen in lane 2 is either missing or strongly attenuated in lane 8. **(B)** ^{1}H, ^{15}N HSQC spectra of ^{15}N Rpn1$_{412-625}$ (black) and with equimolar Dsk2^{UBL} (orange). Rpn1 T1 signals that shift away from their unbound state following the addition of Dsk2^{UBL} domain are labeled.

Although fig. S26 clearly indicates that T1 is a Dsk2-binding site, there may be an alternative Rpn1-binding site for Dsk2 that is encompassed by amino acids 196-369 (18). We observed a defect in Rad23 association with the proteasome with endogenous material (Figure 4E), but in the case of Dsk2, this experiment is complicated by the high off rate (0.165 sec^{-1}) of Dsk2 from Rpn1 (*18*). Consequently, there could be significant association to the T1 site in cells that cannot be observed with endogenous material because Dsk2 dissociation occurs in the control WT sample during proteasome purification. This problem is even worse in the case of the UBL-UBA protein Ddi1 (*18*). Further studies will be required to resolve these issues.

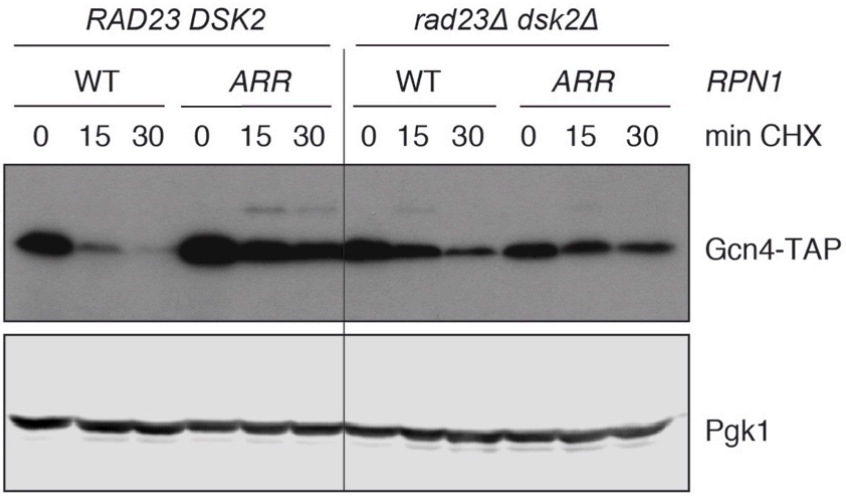

Fig. S27

The T1 site of Rpn1 participates in Gcn4 degradation *in vivo*. *rpn10-uim rpn13-pru* yeast strains bearing TAP-tagged GCN4 integrated at the endogenous chromosomal locus, and other mutations as indicated, were incubated in cycloheximide (CHX) for the indicated times. Lysates were prepared, resolved by SDS-PAGE, blotted, and probed for Gcn4-TAP. Pgk1 serves as a loading control**.**

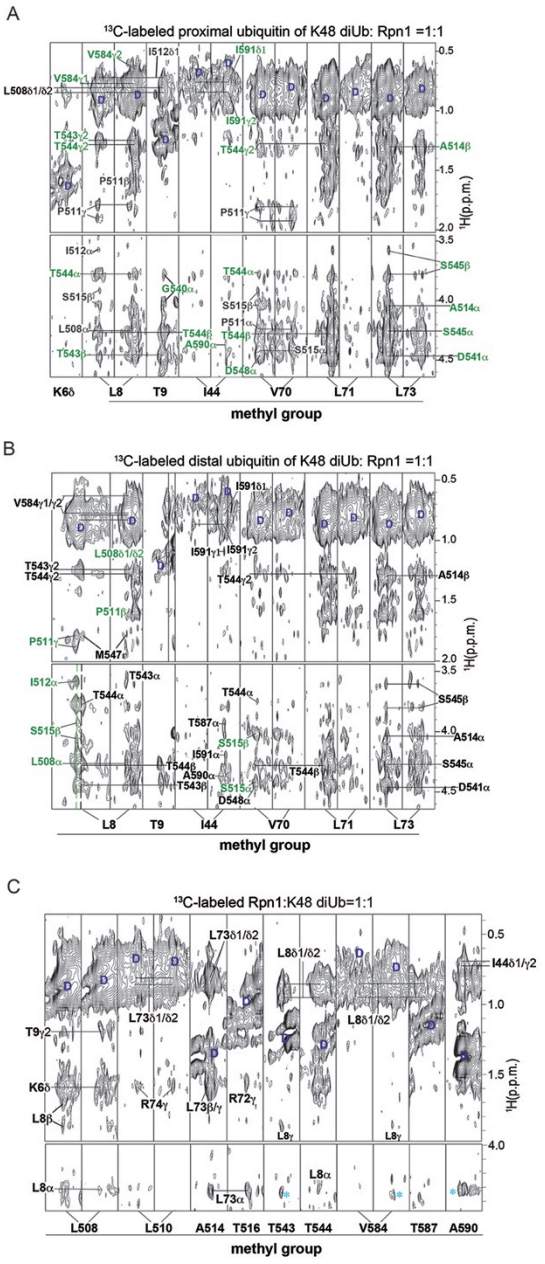

Fig. S28

NOESY spectra record abundant intermolecular NOEs between the Rpn1 T1 site and K48-linked diubiquitin. Intermolecular NOE interactions from half-filtered ^{1}H, ^{13}C NOESY experiments detected for unlabeled $Rpn1_{412-625}$ and K48-linked diubiquitin with proximal **(A)** or distal **(B)** ubiquitin ^{13}C labeled, or for ^{13}C labeled $Rpn1_{412-625}$ and unlabeled K48-linked diubiquitin **(C)**. Breakthrough diagonal peaks are indicated (blue 'D'). Two sets of observed NOE interactions between the Rpn1 T1 site and K48 diubiquitin are labeled in black and green. Signals that were also observed in a control ^{13}C-half-filtered 3D NOESY experiment acquired on free ^{13}C-labeled $Rpn1_{412-625}$ sample

are labeled (light blue asterisks); these are breakthrough peaks from intramolecular NOEs.

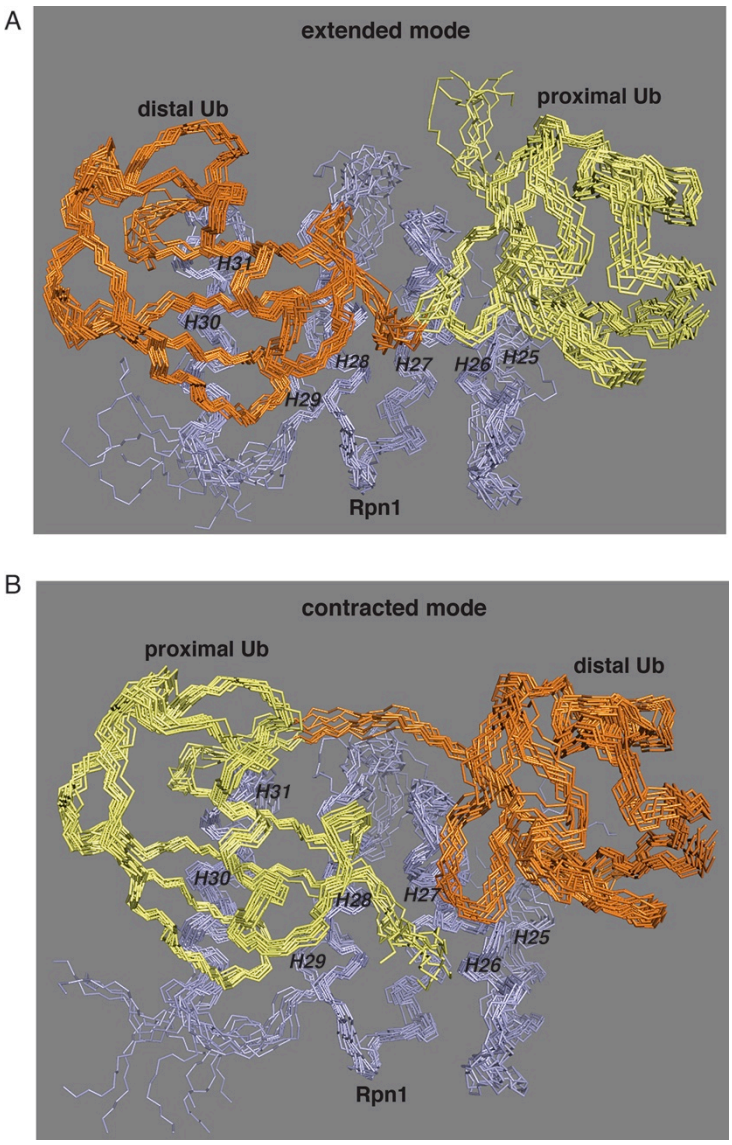

Fig. S29.

Structures of the Rpn1 T1 site complexed with K48-linked diubiquitin. Backbone traces for the ten lowest energy Rpn1 T1:K48-linked diubiquitin structures from 50 linear starting structures with superimposed secondary structure for the extended **(A)** or contracted **(B)** binding mode. $Rpn1_{482-612}$, blue; distal ubiquitin, orange; proximal ubiquitin, yellow. These structures were calculated from the data summarized in Table S2. Briefly, intermolecular distance constraints were used as determined by ^{13}C-half-filtered 3D NOESY experiments on samples of ^{13}C-labeled $Rpn1_{412-625}$:unlabeled K48-linked diubiquitin and of K48-linked diubiquitin with the proximal or distal ubiquitin ^{13}C-labeled mixed with equimolar unlabeled $Rpn1_{412-625}$. PRE-derived intermolecular distance constraints were also used. Intramolecular constraints for $Rpn1_{482-612}$ were used from $^{15}N/^{13}C$ NOESY acquired on $^{15}N/^{13}C$-labeled $Rpn1_{412-625}$:K48-linked diubiquitin as well as from 4D methyl–methyl HMQC-NOESY-HMQC experiments (fig. S13A (right

panel) and S13C). Published constraints were used for ubiquitin (PDB: 1D3Z), as its structure was unchanged.

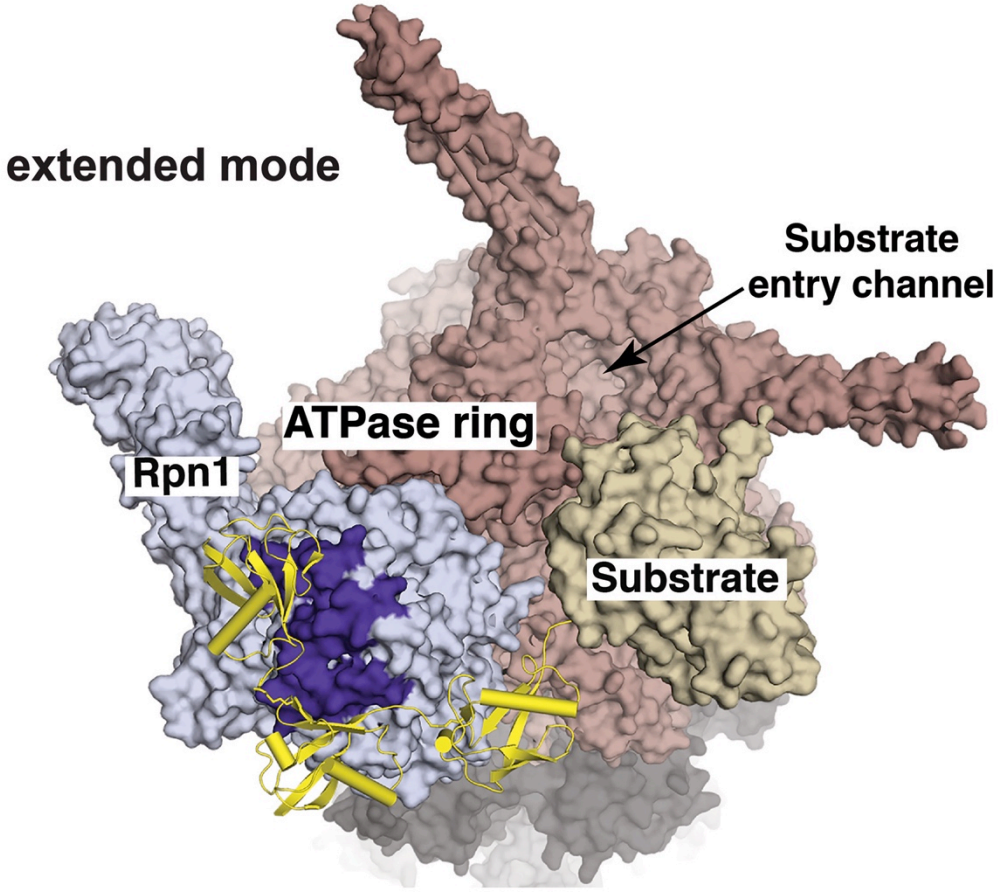

Fig. S30.

Model of K48 triubiquitin bound to the Rpn1 T1 site for the extended binding mode in the context of proteasome ATPase ring. This image was generated by using the Rpn1 T1:K48 diubiquitin structure from Figure 5A and cryoEM-based coordinates (PDB 4CR2). Cyclin B (PDB 2B9R) was used as the model substrate (beige). The ATPase ring is displayed in pink, the CP α-ring in dark grey, and CP β-ring in light grey.

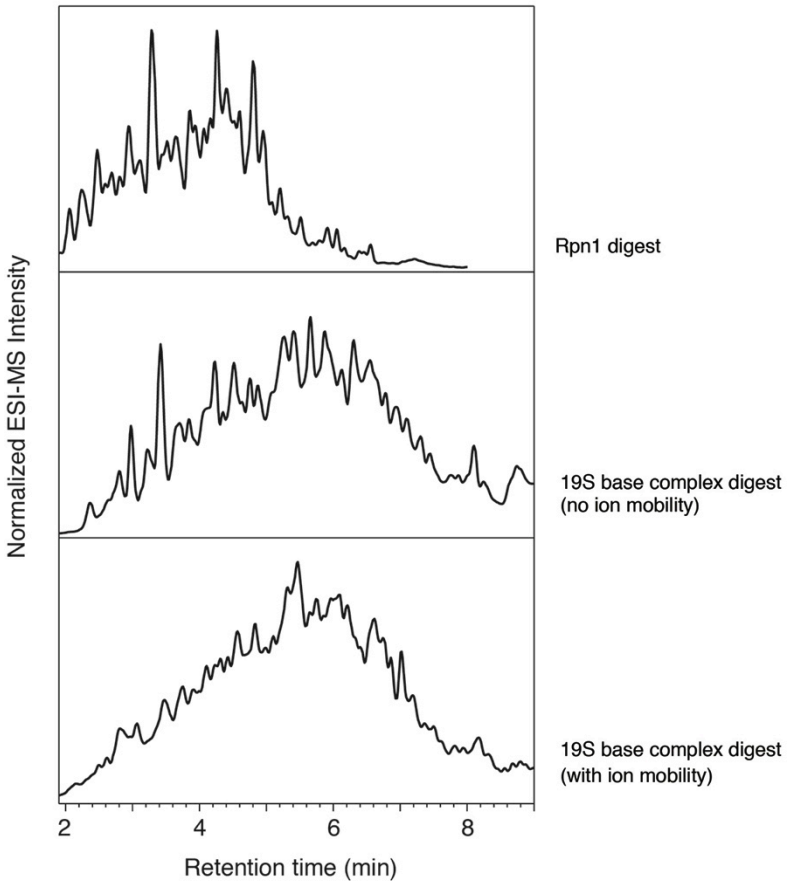

Fig. S31.

Ion mobility spectrometry allows for greater peptide separation of the base complex digest. Recombinant Rpn1 (top panel) was separated via UPLC using a linear 6 min gradient while base samples (middle, bottom panels) used linear 9 min gradients. All analyses employed MSE data-independent acquisition. Further peptide separation of the base complex digest was accomplished by leveraging the ion mobility capabilities of the SYNAPT G2Si mass spectrometer (bottom panel).

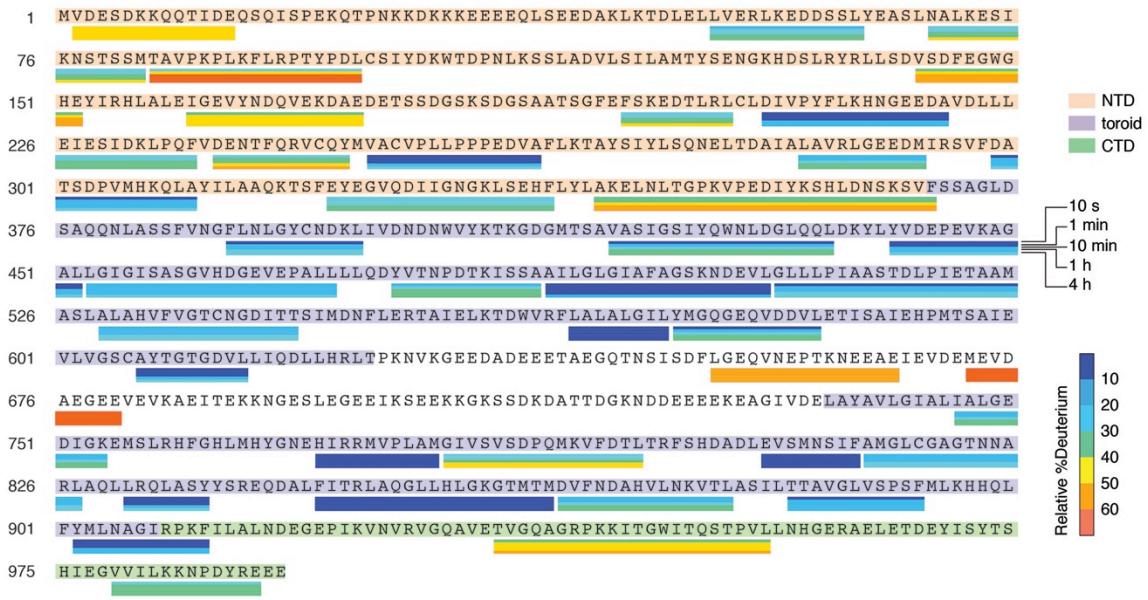

Fig. S32.

Rpn1 is conformationally stable within the context of the base complex. Deuterium uptake for Rpn1 peptides (solid lines below the sequence) derived from pepsin digestion of the base complex was measured at various time points from 10s to 4 h. The amount of deuterium incorporation in each peptide is indicated according to the color scheme at right. Rpn1 domain architecture is color coded as in Figs. 6A and S4A.

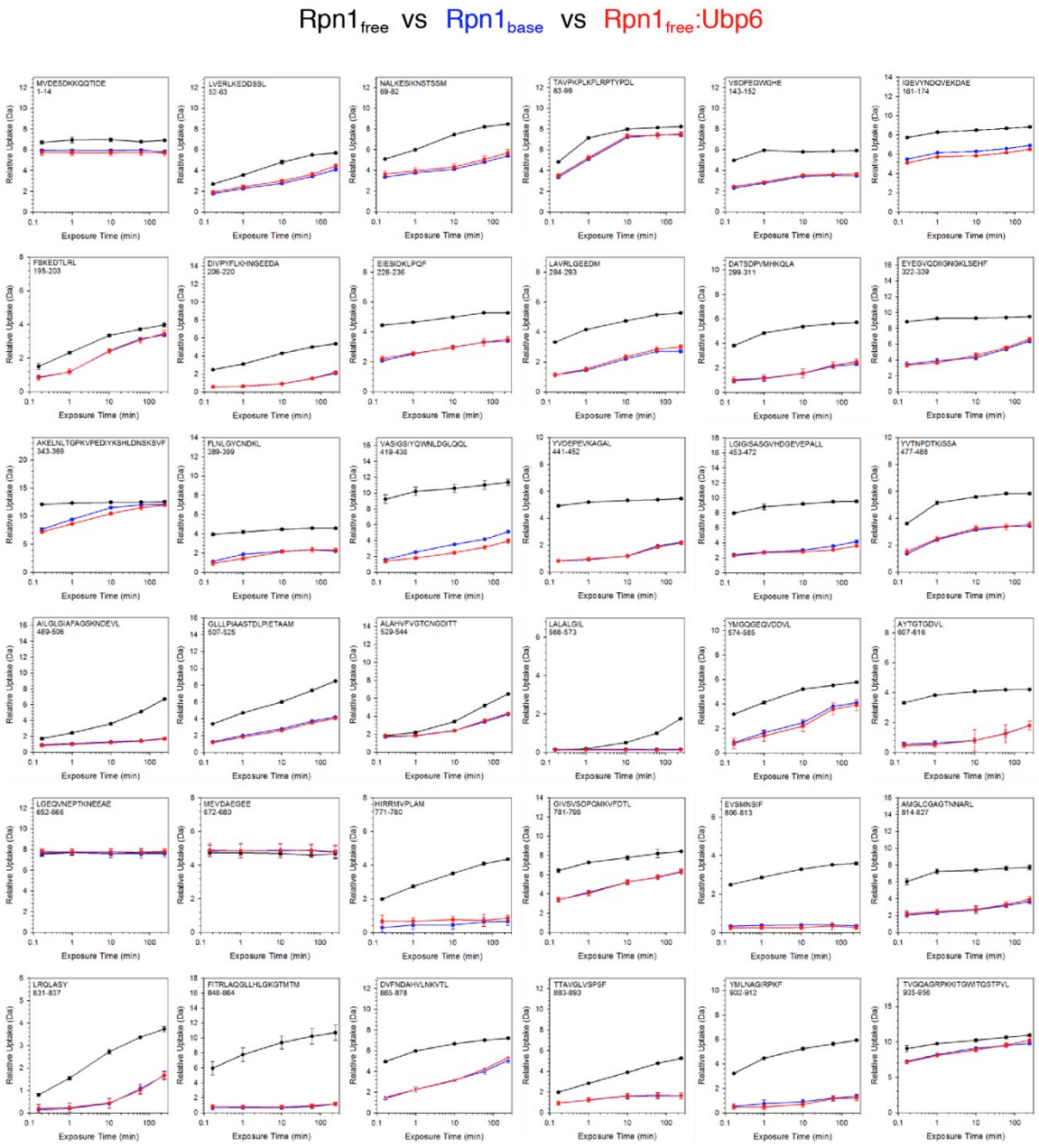

Fig. S33.

Ubp6 binding to the base complex induces highly localized stabilization in Rpn1. Temporal deuterium uptake was plotted for Rpn1 peptides resulting from digestion of recombinant Rpn1 (black), the base complex (blue), and Ubp6-bound base complex (red). Differences in the measured values were calculated according to Eq. 6 (Supplemental methods) and plotted in Figs. 6A and 6B.

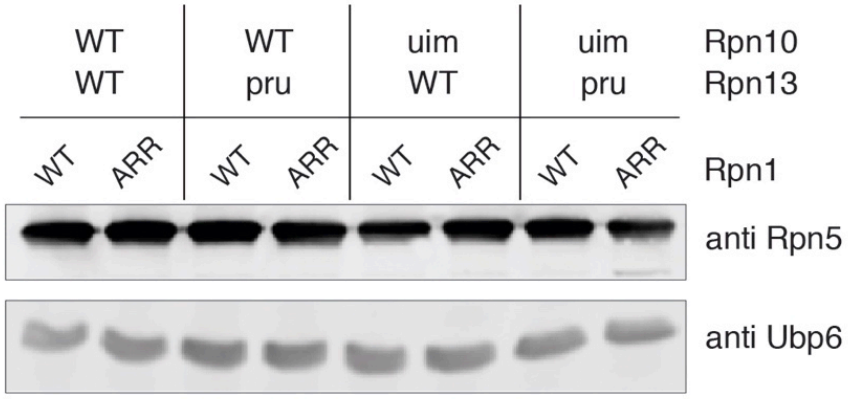

Fig. S34.

Ubp6 interaction with the proteasome does not require the Rpn1 T1 site, the Rpn10-UIM site, or the Rpn13 PRU site. Proteasomes were purified from strains bearing all combinations of intrinsic ubiquitin receptor mutations. Washes prior to elution included 100 mM NaCl, creating more stringent conditions for Ubp6 association. Purified material was resolved by 10% SDS-PAGE, blotted, and probed with antibodies to Ubp6. Rpn5 was probed as a loading control.

Table S1.

Structural statistics for the Rpn1 T1 site.

	$Rpn1_{482-612}$
NMR distance and dihedral constraints	
Distance constraints	
Total NOE	1242
Intra-residue	576
Inter-residue	666
Sequential ($\|i-j\|=1$)	178
Medium-range ($\|i-j\|\leq 4$)	241
Long-range ($\|i-j\|>5$)	247
Hydrogen bonds	59
Total dihedral angle restraints	182
ϕ (°)	91
ψ (°)	91
Structure statistics[§]	
Ramachandran plot (%)	
Most-favorable region	94.6
Additionally allowed region	4.7
Generously allowed region	0.7
Disallowed region	0
RMSD from Average Structure (Å)	
Backbone	0.80 ± 0.14
Heavy	1.32 ± 0.21

[§]Statistics for the II° structural elements of $Rpn1_{482-612}$ for the region spanning H26-H31.

Table S2.
Structural Statistics for Rpn1 T1:ubiquitin and Rpn1 T1:K48 diubiquitin.

	$Rpn1_{482-612}$:ubiquitin		$Rpn1_{482-612}$:K48 diubiquitin	
	site1 (H28/H30)	site2 (H26)	extended	contracted
Intermolecular NOE	80	26	104	100
Intermolecular PRE	18	6	19	8
Intramolecular NOE				
$Rpn1_{482-612}$	1310		1310	
ubiquitin/K48 diubiquitin*	2386		4772	
Hydrogen bonds				
$Rpn1_{482-612}$	59		59	
ubiquitin/K48 diubiquitin*	27		54	
Total dihedral angle restraints				
$Rpn1_{482-612}$	155		155	
ubiquitin/K48 diubiquitin*	47		94	
Structure statistics[§]				
Ramachandran plot (%)				
Most-favorable region	86.0		85.2	85.6
Additionally allowed region	13.0		13.5	13.6
Generously allowed region	1.0		1.3	0.8
Disallowed region	0.0		0.0	0.0
RMSD from Average Structure (Å)				
Backbone	0.58 ± 0.12	0.74 ± 0.27	0.84 ± 0.16	0.80 ± 0.16
Heavy	1.08 ± 0.17	1.25 ± 0.27	1.28 ± 0.20	1.25 ± 0.19

*Taken from PDB 1D3Z

[§]Statistics for the II° structural elements of $Rpn1_{482-612}$ for the region spanning H26-H31 and ubiquitin.

Table S3.
Yeast Strains

All yeast strains are isogenic to SUB61 or SUB62, both of which have the genotype *lys2-801 leu2-3, 2-112 ura3-52 his3Δ200 trp1-1 1.*

Strain	Genotype	Figure
SUB62	*MATa*	1A, 4G
YSS794a	*MATa rpn10-uim::kanMX rad23::hphMX dsk2::CaURA3MX ddi1::LEU2MX*	1A
YSS786a	*MATa rpn13-pru::natMX rpn10-uim::kanMX rad23::hphMX dsk2::CaURA3MX ddi1::LEU2MX*	1A
YSS1101a	*MATa rpn13::natMX rpn10-uim::kanMX rad23::hphMX dsk2::CaURA3MX ddi1::LEU2MX*	1A
YSS366a	*MATa RPN11-TEV-ProA::HIS3 rpn13-pru::natMX rpn10-uim::kanMX*	1B
SDL135	*MATa PRE1-TEV-ProA::HIS3*	1B, 4A, 4B
YSS865a	*MATa RPN11-TEV-ProA::HIS3 RPN1-WT::TRP1 rpn13-pru::natMX rpn10-uim::kanMX*	4A, 4E
YSS869a	*MATα RPN11-TEV-ProA::HIS3 rpn1-ARR::TRP1 rpn13-pru::natMX rpn10-uim::kanMX*	4A, 4E
YSS884a	*MATa RPN1-WT::TRP1 rad23::hphMX dsk2::CaURA3MX ddi1::LEU2MX*	4C
YSS891a	*MATa rpn1-ARR::TRP1 rad23::hphMX dsk2::CaURA3MX ddi1::LEU2MX*	4C
YSS883a	*MATa RPN1-WT::TRP1 rpn10-uim::kanMX rad23::hphMX dsk2::CaURA3MX ddi1::LEU2MX*	4C
YSS890a	*MATa rpn1-ARR::TRP1 rpn10-uim::kanMX rad23::hphMX dsk2::CaURA3MX ddi1::LEU2MX*	4C
YSS882a	*MATa RPN1-WT::TRP1 rpn13-pru::natMX rad23::hphMX dsk2::CaURA3MX ddi1::LEU2MX*	4C
YSS889a	*MATa rpn1-ARR::TRP1 rpn13-pru::natMX rad23::hphMX dsk2::CaURA3MX ddi1::LEU2MX*	4C
YSS881d	*MATa RPN1-WT::TRP1 rpn13-pru::natMX rpn10-uim::kanMX rad23::hphMX dsk2::CaURA3MX ddi1::LEU2MX*	4C
YSS888a	*MATa rpn1-ARR::TRP1 rpn13-pru::natMX rpn10-uim::kanMX rad23::hphMX dsk2::CaURA3MX ddi1::LEU2MX*	4C
YSS913a	*MATa RPN11-TEV-ProA::HIS3 RPN1-WT::TRP1 rpn13-pru::natMX rpn10-uim::kanMX rad23::hphMX dsk2::CaURA3MX ddi1::LEU2MX*	4B, 4D, 7B
YSS914a	*MATa RPN11-TEV-ProA::HIS3 rpn1-ARR::TRP1 rpn13-pru::natMX rpn10-uim::kanMX rad23::hphMX dsk2::CaURA3MX ddi1::LEU2MX*	4B, 4D, 7B
YSS1155d	*MATa RPN11-TEV-ProA::HIS3 rpn1-ARR::TRP1 rpn13-pru::natMX rad23::hphMX dsk2::CaURA3MX ddi1::LEU2MX*	4D, 7B
YSS1158a	*MATa RPN11-TEV-ProA::HIS3 rpn1-ARR::TRP1 rpn10-uim::kanMX rad23::hphMX dsk2::CaURA3MX ddi1::LEU2MX*	4D, 7B
YSS868a	*MATa RPN11-TEV-ProA::HIS3 RPN1-WT::TRP1*	4E
YSS872a	*MATa RPN11-TEV-ProA::HIS3 rpn1-ARR::TRP1*	4E

Table S3.
Yeast Strains

Strain	Genotype	Figure
YSS992a	*MATa RPN1-WT::TRP1 rpn13-pru::natMX rpn10-uim::kanMX rad23::hphMX dsk2::CaURA3MX GIC2-TAP::HIS3*	4F
YSS994a	*MATa rpn1-ARR::TRP1 rpn13-pru::natMX rpn10-uim::kanMX rad23::hphMX dsk2::CaURA3MX GIC2-TAP::HIS3*	4F
YSS984a	*MATa RPN1-WT::TRP1 rpn13-pru::natMX rpn10-uim::kanMX GIC2-TAP::HIS3*	4F
YSS986a	*MATa rpn1-ARR::TRP1 rpn13-pru::natMX rpn10-uim::kanMX GIC2-TAP::HIS3*	4F
YSS857a	*MATa RPN1-WT::TRP1 rpn13-pru::natMX rpn10-uim::kanMX*	4G
YSS857d	*MATα RPN1-WT::TRP1 rpn13-pru::natMX rpn10-uim::kanMX*	4G
YSS861a	*MATa rpn1-ARR::TRP1 rpn13-pru::natMX rpn10-uim::kanMX*	4G
YSS861d	*MATα rpn1-ARR::TRP1 rpn13-pru::natMX rpn10-uim::kanMX*	4G
SUB61	*MATα*	4G
SY1689c	*MATα RPN11-TEV-ProA2::HIS3*	7A
SY1689d	*MATα RPN11-TEV-ProA2::HIS3*	6C, 6D
SY1690b	*MATα RPN11-TEV-ProA2::HIS3 rpn1-D431Y-Q434Y::TRP1*	6C
SY1691b	*MATα RPN11-TEV-ProA2::HIS3 rpn1-D431Y-Q434Y::TRP1*	6C
SY1692b	*MATα RPN11-TEV-ProA2::HIS3 rpn1-L430A-D431A-Q434A-Q435A::TRP1*	6C
SY1693b	*MATα RPN11-TEV-ProA2::HIS3 rpn1-L430A-D431A-Q434A-Q435A::TRP1*	6C
SY1694b	*MATα RPN11-TEV-ProA2::HIS3 rpn1-AKAA::TRP1*	6C, 6D
SY1695b	*MATα RPN11-TEV-ProA2::HIS3 rpn1-AKAA::TRP1*	6C
SY1214	*MATa ProA-TEV-Rpt1::HIS3 rpn13-pru::natMX rpn10-uim::kanMX*	7A, S3
SY1210	*MATa ProA-TEV-Rpt1::HIS3 rpn1-ARR::TRP1 rpn13-pru::natMX rpn10-uim::kanMX*	7A
SY1724	*MATa ProA-TEV-Rpt1::HIS3 rpn1-AKAA::TRP1 rpn13-pru::natMX rpn10-uim::kanMX*	7A

Table S3.
Yeast Strains

Strain	Genotype	Figure
SY1702a	*MATα RPN11-TEV-ProA::HIS3 ubp6::URA3 rpn13-pru::natMX rpn10-uim::kanMX sem1::hphMX*	S2
SY1704a	*MATα RPN11-TEV-ProA::HIS3 ubp6::URA3 rpn13-pru::natMX rpn10-uim::kanMX*	S2
SY1703a	*MATα RPN11-TEV-ProA::HIS3 ubp6::URA3 rpn10-uim::kanMX sem1::hphMX*	S2
SY1705a	*MATα RPN11-TEV-ProA::HIS3 ubp6::URA3 rpn10-uim::kanMX*	S2
YSS913c	*MATa RPN11-TEVProA::HIS3 RPN1-WT::TRP1 rpn13-pru::natMX rpn10-uim::kanMX rad23::hphMX dsk2::CaURA3MX ddi1::LEU2MX*	S22A, S22B
YSS914l	*MATa RPN11-TEVProA::HIS3 rpn1-ARR::TRP1 rpn13-pru::natMX rpn10-uim::kanMX rad23::hphMX dsk2::CaURA3MX ddi1::LEU2MX*	S22A, S22B
YSS913a	*MATa RPN11-TEVProA::HIS3 RPN1-WT::TRP1 rpn13-pru::natMX rpn10-uim::kanMX rad23::hphMX dsk2::CaURA3MX ddi1::LEU2MX*	S22A, S22B, S23D
YSS914a	*MATa RPN11-TEVProA::HIS3 rpn1-ARR::TRP1 rpn13-pru::natMX rpn10-uim::kanMX rad23::hphMX dsk2::CaURA3MX ddi1::LEU2MX*	S22A, S22B, S23D
YSS884a	*MATa RPN1-WT::TRP1 rad23::hphMX dsk2::CaURA3MX ddi1::LEU2MX*	S22C
YSS891a	*MATa rpn1-ARR::TRP1 rad23::hphMX dsk2::CaURA3MX ddi1::LEU2MX*	S22C
YSS883a	*MATa RPN1-WT::TRP1 rpn10-uim::kanMX rad23::hphMX dsk2::CaURA3MX ddi1::LEU2MX*	S22C
YSS890a	*MATa rpn1-ARR::TRP1 rpn10-uim::kanMX rad23::hphMX dsk2::CaURA3MX ddi1::LEU2MX*	S22C
YSS882a	*MATa RPN1-WT::TRP1 rpn13-pru::natMX rad23::hphMX dsk2::CaURA3MX ddi1::LEU2MX*	S22C
YSS889a	*MATa rpn1-ARR::TRP1 rpn13-pru::natMX rad23::hphMX dsk2::CaURA3MX ddi1::LEU2MX*	S22C
YSS881a	*MATa RPN1-WT::TRP1 rpn10-uim::kanMX rpn13-KKAAD::natMX rad23::hphMX dsk2::CaURA3MX ddi1::LEU2MX*	S22C
YSS888a	*MATa rpn1-ARR::TRP1 rpn10-uim::kanMX rpn13-KKAAD::natMX rad23::hphMX dsk2::CaURA3MX ddi1::LEU2MX*	S22C
YSS860a	*MATa RPN1-WT::TRP1*	S22D
YSS864a	*MATa rpn1-ARR::TRP1*	S22D
YSS859a	*MATa RPN1-WT::TRP1 rpn10-uim::kanMX*	S22D
YSS863a	*MATa rpn1-ARR::TRP1 rpn10-uim::kanMX*	S22D
YSS858a	*MATa RPN1-WT::TRP1 rpn13-pru::natMX*	S22D
YSS862a	*MATa rpn1-ARR::TRP1 rpn13-pru::natMX*	S22D
YSS857a	*MATa RPN1-WT::TRP1 rpn13-pru::natMX rpn10-uim::kanMX*	S22D
YSS861a	*MATa rpn1-ARR::TRP1 rpn13-pru::natMX rpn10-uim::kanMX*	S22D

Table S3.
Yeast Strains

Strain	Genotype	Figure
YSS865a	*MATa RPN11-TEV-ProA::HIS3 RPN1-WT::TRP1 rpn13-pru::natMX rpn10-uim::kanMX*	S24, S25, S23A, S23C, S34
YSS869a	*MATa RPN11-TEVProA::HIS3 rpn1-ARR::TRP1 rpn13-pru::natMX rpn10-uim::kanMX*	S24, S25, S23A, S23C, S34
SDL135	*MATa PRE1-TEV-ProA::HIS3*	S22D, S24
YSS868a	*MATa RPN11-TEV-ProA::HIS3 RPN1-WT::TRP1*	S25, S34
YSS872a	*MATa RPN11-TEV-ProA::HIS3 rpn1-ARR::TRP1*	S25, S34
YSS867a	*MATa RPN11-TEV-ProA::HIS3 RPN1-WT::TRP1 rpn13-pru::natMX*	S25, S34
YSS871a	*MATa RPN11-TEV-ProA::HIS3 rpn1-ARR::TRP1 rpn13-pru::natMX*	S25, S34
YSS866a	*MATa RPN11-TEV-ProA::HIS3 RPN1-WT::TRP1 rpn10-uim::kanMX*	S25, S34
YSS870a	*MATa RPN11-TEV-ProA::HIS3 rpn1-ARR::TRP1 rpn10-uim::kanMX*	S25, S34
YSS988a	*MATa RPN1-WT::TRP1 rpn13-pru::natMX rpn10-uim::kanMX rad23::hphMX dsk2::CaURA3MX GCN4-TAP::HIS3*	S27
YSS990a	*MATa rpn1-ARR::TRP1 rpn13-pru::natMX rpn10-uim::kanMX rad23::hphMX dsk2::CaURA3MX GCN4-TAP::HIS3*	S27
YSS980a	*MATa RPN1-WT::TRP1 rpn13-pru::natMX rpn10-uim::kanMX GCN4-TAP::HIS3*	S27
YSS982a	*MATa rpn1-ARR::TRP1 rpn13-pru::natMX rpn10-uim::kanMX GCN4-TAP::HIS3*	S27

Table S4.
Antibodies

Antigen	Source	Reference	Secondary antibody information	Working concentration
Rpn5	Finley Lab	(*26*)	rabbit	1:5,000
Rpn1	Finley Lab	this study	rabbit	1:5,000
Ubp6	Finley Lab	this study	rabbit	1:50,000
Rad23	Finley Lab	this study	rabbit	1:5,000
Dsk2	Michael Glickman	(*29*)	chicken	1:1,000
Ddi1	Duncan Clarke	(*72*)	rabbit	1:5,000
Pre6	William Tansey	(*73*)	mouse	1:2,000
Pgk1	Promega	459250	mouse	1:10,000
ubiquitin	Santa Cruz Biotech	sc-8017	mouse	1:1,000
GST	Santa Cruz Biotech	sc-138	mouse	1:10,000
T7 epitope	EMD Millipore	69048-3	HRP-conjugated	1:10,000
Flag epitope	Sigma-Aldrich	F3165	HRP-conjugated	1:5,000
PAP	Sigma-Aldrich	P1291	protein complex with HRP	1:1,000

Table S5.
Plasmids for the expression of recombinant proteins

plasmid name	recombinant protein	N-terminal tag	C-terminal tag	Figure
pUB406	Rpn1	GST	---	1C
YSp274	Rpn1-ARR	GST	---	3C-3D
YSp33	Rpn1-N	GST	---	S4C
YSp105	Rpn1-M	GST	---	S4C
YSp125	Rpn1-C	GST	---	S4C
YSp158	Rpn1-412-625	GST	---	2A
YSp271	Rpn1-412-625-ARR	GST	---	2A
pTXB1-Rpn1	Rpn1	Intein	---	6A-6B
pUB414	Rpn10	GST	---	1C, 3D
pUB417	Rpn10-UIM	GST	---	3C-3D
YSp64	Rpn13	GST	---	1C
YSp308	Rpn13-pru	GST	---	1C
YSp20	Rpn13	GST	---	S1
YSp1	Rpn13-KKD	GST	---	S1
YSp13	Rpn13-KKAAD	GST	---	S1
pBM1d	Dsk2-UBL	GST	---	4D
pRG63	Rad23-UBL	GST	---	4D
YSp103	Rad23ΔUBA	---	FLAG-/Intein	3D
YSp104	Rad23ΔUBLΔUBA	---	FLAG-/Intein	3D
YSp46	Rad23	---	FLAG-/Intein	S23B-S23C
pDL83	Ubp6-UBL	GST	---	7A
pTYB12-Ubp6	Ubp6	Intein	---	7B
pET15b-Ubp6	Ubp6	His	---	6A-6B
pGEX-6P-1-Ubp6	Ubp6	GST	---	6D